Force-dependent recruitment of Piezo1 drives focal adhesion maturation and calcium entry in normal but not tumor cells

Mingxi Yao*[1,2,3], Ajay Tijore[3,4], Delfine Cheng[5], Jinyuan Vero Li[5], Anushya Hariharan[3], Boris Martinac[5], Guy Tran Van Nhieu[6], Charles D Cox*[5] & Michael Sheetz*[3,7,8]

1. Department of Biomedical Engineering, Southern University of Science and Technology
2. Guangdong Provincial Key Laboratory of Advanced Biomaterials
3. Mechanobiology Institute, National University of Singapore Mechanobiology Institute, National University of Singapore
4. Centre for Biosystems Science and Engineering, Indian Institute of Science, Bangalore, 560012, India
5. Victor Chang Cardiac Research Institute
6. Ecole Normale Supérieure PARIS-SACLAY
7. Dept of Biological Sciences, National University of Singapore
8. Molecular MechanoMedicine Program, Dept. of Biochemistry and Molecular Biology, University of Texas Medical Branch

*Correspondence: yaomx@sustech.edu.cn, C.Cox@victorchang.edu.au or misheetz@utmb.edu

Significance Statement

Piezo1 localizes to focal adhesions under force in a cell-state dependent manner and faciliates calcium entry and adhesion matruration/turnover.

Abstract:

Mechanosensing is an integral part of many physiological processes including stem cell differentiation, fibrosis and cancer progression. Two major mechanosensing systems – focal adhesions and mechanosensitive ion channels, can convert mechanical features of the microenvironment into biochemical signals. We report here surprisingly that the mechanosensitive Ca^{2+}-permeable channel Piezo1, previously perceived to be diffusive on plasma membranes, binds to matrix adhesions in a force-dependent manner, promoting adhesion maturation and cell spreading in normal but not in tumor cells. In the absence of Piezo1, matrix adhesions are smaller in normal cells mimicking transformed cells where adhesions do not change with or without Piezo1. A novel adhesion-targeted calcium sensor shows robust Piezo1-dependent, calcium influx at adhesions in

30 normal cells; but not in transformed cells. A linker domain in Piezo1 is needed for binding to adhesions and
31 overexpression of the domain blocks Piezo1 binding to adhesions decreasing adhesion size and cell spread
32 area. Thus, we suggest that Piezo1 is a novel component of focal adhesions in non-transformed cells that
33 catalyzes adhesion maturation and growth through force-dependent calcium signaling, but this function is
34 absent in most cancer cells.

35 *Introduction*

36 Cellular mechanosensing, the cell's ability to detect and respond to its physical microenvironment, is
37 involved in important processes including development, tissue homeostasis and disease(*1*, *2*). For example,
38 sensing of shear flow in blood circulation is essential for the proper development of the vasculature and the
39 depletion of rigidity sensors enables cancer neoplastic transformation, i.e. substrate-rigidity-independent
40 growth(*3*, *4*). Mechanosensitive ion channels and integrin-mediated focal adhesions, are major
41 mechanosensors that are responsible for converting mechanical cues into biochemical signals in these
42 processes(*5*).

43 A mechanosensing function of focal adhesions is manifest by rigidity-dependent adhesion assembly and
44 turnover, which involves hundreds of different focal adhesion proteins that alter cell behavior during
45 spreading and migration(*1*). In addition, focal adhesion mechanosensing regulates pathways such as AKT,
46 MAPK and Hippo-signaling that influence cell fate decisions(*1*, *6*, *7*). Because adhesions affect cell behavior
47 and fate, the molecular components and dynamics of focal adhesions have been extensively studied. There
48 exists a robust process of adhesion protein recruitment and processing in the finely tuned steps of focal
49 adhesion formation, growth and turnover that correlates with cell state decision making based on cell-
50 microenvironment interactions(*8*). There is evidence for force-sensing proteins such as talin and vinculin
51 regulating the functions of focal adhesions as well(*2*, *8*–*13*). In contrast, although the ion conduction
52 properties of many mechanosensitive ion channels are well-characterized by structural and patch-clamp
53 studies, the mechanisms for converting matrix forces to channel gating are not well understood(*14*). This is

54 partly due to the complex nature of ion channel signaling and mechanically-induced calcium influx. For
55 example, mechanosensitive channels are linked to both cell proliferation and apoptosis depending on the
56 context, suggesting that both the distribution and dynamics of the mechanosensitive ion channels are
57 important for understanding the critical mechanosensing processes of the cell(*15*, *16*).

58 There is ample evidence of a crosstalk between mechanosensitive ion channels and focal adhesions. Local
59 calcium entry is critical for focal adhesion assembly and disassembly based upon the calpain dependence of
60 both processes (*17–21*). In adhesion assembly during cell spreading, rigidity sensing involves force-dependent
61 calpain cleavage of talin, which is needed for normal adhesions to form and for normal cells to grow(*20*). In
62 contrast, transformed cells do not sense matrix rigidity and adhesions are significantly smaller even though
63 tumor cells develop higher traction forces(*22*). This raises questions of whether or not transformed cells use
64 calcium in adhesion assembly like normal cells. In addition, several studies found that adhesion disassembly
65 depends upon force-dependent calpain cleavage(*18*, *19*). Thus, there are critical roles for calcium entry in
66 normal adhesion dynamics that are altered in transformed (tumor) cells and the analysis of the channels
67 involved can reveal important aspects of the life cycle of focal adhesions.

68 Several calcium-permeable channels have been implicated in focal adhesions dynamics (*23–27*) . One of those,
69 Piezo1, is particularly interesting, as early reports of Piezo1 document an interaction with integrins(*28*). Piezo1
70 has subsequently been identified as a bona-fide mechanosensitive ion channel in mammalian cells(*29*). Since
71 then, Piezo1 has been shown to have many roles in important biological processes and there is increasing
72 interest in how it functions *in situ*(*15*, *29–31*). Piezo1 is widely expressed in somatic cell types and is linked to
73 mechanosensing in stem cell lineage determination, blood pressure regulation, activation of innate immunity
74 and vascular development(*4*, *30*, *32*, *33*). Piezo1's activity has been shown to be related to the integrin-linked
75 actin cytoskeleton (*26*, *34*, *35*). When Neuro2A cells are mechanically agitated with micron-sized, collagen IV
76 or Matrigel coated beads, the tension threshold required to trigger Piezo-dependent Ca^{2+} entry is significantly
77 reduced(*36*). In addition, integrin signaling pathways are critical for proper function of Piezo1 in the context

78 of endothelial cell responses to flow(*37*). Consequently, we want to investigate the possible crosstalk between
79 Piezo1 and focal adhesions.

80 In this study, we show that in normal cell lines Piezo1 is needed for mature adhesion assembly and it
81 localizes to adhesions as the adhesions mature . In normal cell lines from many tissues, Piezo1 is enriched at
82 focal adhesions in a force-dependent manner and dissociates after the integrin adhesions disassemble. Its
83 localization correlates with local calcium entry and adhesion disassembly likely through a calpain-dependent
84 process[20]. Alternatively, in transformed cells, Piezo1 is diffusely distributed and does not affect either
85 adhesion assembly or disassembly and there is low adhesion calcium entry. These studies indicate that Piezo1
86 normally interacts with adhesions transiently during assembly and then its force-dependent recruitment to
87 mature adhesions catalyzes integrin-specific adhesion disassembly. These dynamic adhesion interactions are
88 lost in transformed cells and are likely a key neoplastic modification.

89 *Results*

90 *Piezo1 stably localizes to mature adhesions in HFF cells*

91 To investigate the role of Piezo1 in adhesion formation, we followed the distribution and dynamics of
92 Piezo1 localization during cell spreading in Human Foreskin Fibroblast (HFF) cells using total internal
93 reflection fluorescence microscopy (TIRFM). Transiently expressed Piezo1 tagged with GFP(*38*) or mRuby3
94 and paxillin-BFP were followed during the cell spreading in HFF cells (Figure 1A top panel, supplementary
95 movie 1). In the initial phase of spreading, Piezo1 did not colocalize with cell adhesions marked by paxillin
96 and it appeared concentrated around the nucleus. After 30-60 minutes when the cells developed mature
97 adhesions, Piezo1 dispersed to the entire spread area of the cell and was significantly enriched in maturing
98 adhesions.

99 Piezo1 localization to adhesions increased over time until the cell began to polarize. Upon cell
100 polarization, Piezo1 prominently localized to the retracting edges (Figure 1B, upper panel). After spreading

101 overnight, HFF cells reached a dynamic steady state and Piezo1 was enriched at mature focal adhesions
102 (Figure 1B, middle panel). In most cells, Piezo1 was recruited to a sub population of the focal adhesions,
103 mostly around the cell periphery at the ends of stress fibers. Quantification of the extent of Piezo1
104 recuitment to focal adhesions by the ratio of Piezo1 intensity in the adhesion to that in the plasma
105 membrane background showed that the recruitment of Piezo1 to adhesions increased over time as cells
106 spread further and started to polarize (Figure 1 C-D). Piezo1 was often recruited to a portion of individual
107 adhesions as well (Figure 1B lower panel, marked by arrow), implying that the regulation of Piezo1
108 recruitment happened locally. The localization of endogenous Piezo1 to adhesions in HFF cells was also
109 observed by Piezo1 immunostaining of fixed HFF cells (Figure S1) using two knockdown/knockout validated
110 antibodies(*15*). Thus, Piezo1 complexed with mature and retracting adhesions in polarized cells on
111 fibronectin.

112 Since Piezo1 was previously reported to be diffusive in plasma membranes(*26*), we confirmed that the
113 Piezo1 recruitment involved immobilization by checking the lifetime of Piezo1 in the focal adhesions of HFF
114 cells through Fluorescence Recovery After Photobleaching (FRAP). Surprisingly, as shown in Figure 1E, Piezo1
115 was stable at the adhesions after recruitment, with lifetimes of around 120 s that were considerably longer
116 compared to typical focal adhesion proteins such as paxillin ~25 s and even slightly longer than integrins
117 such as integrin β3 ~90 s (Figure 1F). In addition, the mobile fraction of Piezo1 was considerably less than the
118 mobile fraction of paxillin and even integrin β3 (Figure 1F). These data indicated that Piezo1 formed stable
119 interactions with certain focal adhesion components in HFF cells.

120 *Piezo1 recruitment to adhesions requires myosin II contractility*

121 Since focal adhesion maturation was linked to sustained traction forces and correlated with Piezo1
122 recruitment during spreading, we hypothesized that Piezo1-adhesion interactions were force dependent.
123 Treatment of Piezo1-GFP expressing HFF cells with 30 μM of Y-27632 to inhibit actomyosin contraction,
124 caused rapid loss of Piezo1 from adhesion sites and was followed by the disassembly of focal adhesions as
125 measured by paxillin (Figure 2A, top panel, supplementary movie2). Similar results were observed with 50

126 μM blebbistatin treatment (Figure S2A). When Y-27632 was washed out, Piezo1 returned rapidly to the
127 reforming adhesions (Figure 2A, top panel). Since Piezo1 recruitment during recovery was much more rapid
128 than the initial recruitment to adhesions during cell spreading (minutes versus hours), we postulated that
129 components remaining at adhesions in the absence of force catalyzed the rapid recovery of adhesion
130 proteins with the development of contractile forces to enable Piezo1 binding. Further, when the
131 contractility of the cell was enhanced by co-expressing the constitutively active version of RhoA along with
132 Piezo1 in HFF cells, the enrichment of Piezo1 at adhesions was strongly promoted (Figure 2A, bottom panel).

133 To check whether the reduction of traction forces alone could disrupt Piezo1's adhesion recruitment
134 without disruption of adhesion proteins such as talin and integrins, we tested the relationship between
135 Piezo1 localization and myosin II contractility in intact adhesions. Previous reports showed that inhibition of
136 the tyrosine phosphatase, PTP-PEST, as well as the expression of virulence bacterial protein IpaA, inhibited
137 adhesion disassembly upon addition of Y-27632 (*39*, *40*). In cells expressing GFP-labelled IpaA peptide,
138 addition of 30 μM Y-27632 caused cells to lose contractility while retaining adhesion structures (Figure 2B,
139 Supplemental movie 3). In this case, Piezo1-mRuby3 diffused out from adhesions within 10 min after Y-
140 27632 addition while the integrin β3-BFP remained intact. A similar effect was observed when 2.5 μM of
141 PTP-PEST inhibitor was added in combination with 30 μM Y-27632 (Figure S2B). Thus, the localization of
142 Piezo1 to focal adhesions depended on continued contraction forces possibly through the stretching of
143 adhesion proteins, and was independent of paxillin or integrin β3 localization to adhesions.

144 To further establish the role of myosin II-based contractility in Piezo1 recruitment, we checked the
145 distribution of Piezo1 in cells that had low traction forces such as COS-7 cells lacking myosin IIA
146 expression(*41*). In COS-7 cells transiently expressing Piezo1-GFP and paxillin-mapple, Piezo1 was diffusive in
147 the membrane with no apparent localization to adhesions (Figure 2C, top panel) and the cell adopted a
148 highly-spread disc morphology. When contractility was restored in COS-7 cells by overexpressing myosin IIA,
149 cells became polarized with myosin IIA forming stress-fiber-like cables (Figure 2C, bottom panel) and Piezo1

150 was recruited to the adhesions at the ends of the myosin cables. This further reinforced the hypothesis that
151 Piezo1 recruitment to adhesions required continued force on the adhesion complex.

152 *Piezo1 recruitment triggers integrin β3 adhesion turnover*

153 Since Piezo1 was recruited to only a fraction of focal adhesions, we proceeded to check whether different
154 integrin subtypes played a role in the regulation of Piezo1 localization. As shown in Figure 3A, we transiently
155 expressed Piezo1-1591-mRuby3 with integrin β3-mEmerald and analyzed the colocalization of Piezo1 with β3
156 adhesions during cycles of adhesion assembly and disassembly. Interestingly, the recruitment of Piezo1 to β3-
157 enriched adhesions correlated with the disassembly and turnover of the β3 adhesions. Figure 3A shows the
158 timelapse views of two such turnover events on fibronectin surfaces, one during spreading where the cell was
159 protruding and the other in migrating cells where the adhesion was retracting. In both cases, integrin β3-
160 based adhesions formed without apparent Piezo1 co-localization. Over time, Piezo1 was recruited to the
161 adhesions from the periphery of the adhesions and gradually occupied the whole adhesion. Piezo 1
162 recruitment appeared to initiate a decrease in integrin β3 fluorescence intensity within minutes (Figure 3A-B,
163 Figure S3A and supplementary movie 4-6). After integrin β3 reached background levels, the Piezo1
164 fluorescence often persisted in adhesions for a few minutes before dissociation (Figure 3A-B, marked by
165 arrows; and Figure 3 D for kymograph), suggesting that some adhesion components remained that supported
166 Piezo1 localization after integrin β3 dissociated from the adhesion.

167 In contrast, the anticorrelated behavior was not observed between Piezo1 and β1 integrins in adhesions.
168 Piezo1 recruitment at integrin β3 and β1 enriched adhesions was more stable, and they often co-localized for
169 tens of minutes ((Figure 3C, 3E for kymograph). In another interesting example (Figure S3B), Piezo1
170 recruitment correlated with the rapid dissociation of β3 integrins and enrichment of β1 integrins. Piezo1
171 recruitment persisted in adhesions even after dissociation of β3 integrins (Fig. S3B, arrows). These
172 observations indicated that Piezo1 recruitment was associated with adhesion turnover that was regulated
173 locally in an integrin β3 dependent manner. Considering Piezo1's function as a mechanosensitive Ca^{2+} channel,
174 adhesion turnover is likely caused by the calpain-dependent cleavage pathway. Based upon these findings we

175 hypothesized that Piezo1 recruitment was upstream of calpain in regulating adhesion turnover. In earlier
176 studies of cells on fibronectin, integrin β3 adhesions formed initially, and then the adhesions switched to
177 integrin β1. The greater stability of β1-containing adhesions with Piezo1 recruitment could potentially provide
178 a mechanistic explanation for such switching events(*42*).

179

180 *Piezo1 localization to adhesions is lost in transformed cells*

181 To check whether Piezo1 localization to adhesions was cell-type specific, we expressed Piezo1 in a variety
182 of normal and transformed cell lines (Figure 4A, Figure S4A). In all of the normal cell lines of fibroblastic (HFF,
183 MCF-10A), epithelial (HUMEC) or endothelial origins (HUVEC), Piezo1 localized to a significant subset of the
184 focal adhesions on fibronectin demarcated by paxillin (Figure 4A-B, Figure S4). In the case of 12 different
185 tumor cell lines from mesenchymal or epithelial tissues (fibrosarcoma, melanoma, breast and lung cancers,
186 Figure 4B-D), there was no significant colocalization of Piezo1 with paxillin containing adhesions. In the
187 HT1080 (fibrosarcoma) and MDA-MB-231 (breast cancer) cells, FRAP measurements of Piezo1 diffusion
188 showed that Piezo1 had a significantly higher mobile fraction than in HFF cells (Figure 4C). The difference in
189 Piezo1 immobilization was not due to absence of Piezo1 expression, since Western blots confirmed significant
190 Piezo1 expression in most transformed cell lines (Figure 5C, Figure S4B). Thus, the colocalization of Piezo1 with
191 adhesions was found only in normal cells. In all of the tumor cells tested, Piezo1 was not colocalizing with
192 adhesions and was rapidly diffusing.

193 Our previous studies showed that TPM 2.1 levels were low in many transformed cells(*22*). Knocking
194 down TPM 2.1 in HFF cells caused the cells to become transformed with smaller adhesions and the cells
195 were not able to differentiate between soft and rigid surfaces. In contrast, restoring TPM 2.1 expression in
196 MDA-MB-231 cells caused normal behavior with bigger adhesions and the cells died on soft agar(*22*). Based
197 on this, we checked if toggling between the non-transformed and transformed states in HFF and MDA-MB-
198 231 cells altered the localization of Piezo1 in these cell lines. When we knocked down TPM 2.1 in HFF cells,

199 the recruitment of Piezo1 to adhesions was significantly weakened compared with control cells or control
200 siRNA-treated cells (Figure S5A). In contrast, when we transiently expressed TPM 2.1-YFP in MDA-MB-231
201 cells, a fraction of cells formed stress fibers and Piezo1 was recruited to adhesions at the end of stress fibers
202 (Figure S5B). These data indicated that there was a correlation between normal cell behavior and Piezo1
203 adhesion localization and we recently showed that transformation resulted from the loss of rigidity sensing,
204 which was observed in the majority tumor cells(*22*). Thus, the change in cell state from normal to
205 transformed state diminished Piezo1 binding to adhesions.

206 *Piezo1 is needed for adhesion maturation and polarity in normal but not in*
207 *transformed cells*

208 As the pattern of Piezo1 adhesion recruitment differs in normal and transformed cell lines, we checked if
209 Piezo1 regulated focal adhesion morphology differently in normal and transformed cell lines. To minimize
210 the possibility of cell-type variance, we used normal primary cells and transformed cancer cells of matching
211 origin (Human foreskin fibroblast with HT1080 human fibrosarcoma). As shown in Figure 5A, Piezo1 knock-
212 down HFF cells spread to smaller areas, had a lower aspect ratio and had smaller adhesions, while in the
213 transformed HT1080 cells, knocking down of Piezo1 caused a significant increase in cell spread area but had
214 no effect on aspect ratio or adhesion size (Figure 5 A-C).

215 This indicated that Piezo1 was important for adhesion maturation and cell polarization in normal cells
216 but had little effect on adhesion formation in transformed cells, while affecting spreading area. Previous
217 studies documented that transformed cell lines including cancer cells generally had smaller and less mature
218 adhesions compared with non-transformed cells(*22*, *43*). This was despite the fact that the majority of
219 adhesion components were present at similar levels in both normal and transformed cells(*44*, *45*). Thus,
220 Piezo1 recruitment to adhesions in normal cells appeared to be involved in important steps in the adhesion
221 maturation process whereas in transformed cells, Piezo1 depletion caused no change in adhesion
222 morphology(*46*).

223 *Piezo1's adhesion recruitment leads to local calcium transients around adhesions in*
224 *normal but not in transformed cells.*

225 Next we checked the possible physiological significance of the Piezo1 adhesion recruitment. Since Piezo1
226 functions as a mechanosensitive ion channel, the recruitment of Piezo1 to adhesions may have altered the
227 calcium entry pattern of the cells. Recent studies by Ellefsen et. al, showed that Piezo1-dependent calcium
228 spikes were localized to the cell periphery near focal adhesions(*26*). This implied that calcium spikes
229 occurred near where there were concentrations of Piezo1 at adhesions. Because Piezo1 was not
230 concentrated in adhesions of transformed cells such as MDA-MB-231 and HEK293T, there was a question of
231 whether or not similar calcium spikes would occur near adhesions in transformed cells.

232 To determine if calcium entry near adhesions in fibroblasts also occurred in tumor cells, we loaded HFF
233 and MDA-MB-231 cells with the cell-permeable calcium indicator Cal-520 and imaged transient calcium
234 "puffs" on fibronectin surfaces. Similar to previous observations in HFF cells(*26*) , many local calcium entry
235 events were detected in areas of high contractility at the cell edge and surrounding adhesions (Figure S6).
236 Interestingly, although the transformed MDA-MB-231 cells generated higher local traction forces(*22*) and
237 were killed by calcium-dependent apoptosis after stretch(*16*), they had very few calcium spikes on
238 fibronectin surfaces (Figure S6). This indicated that the calcium influx in cancer cells was abnormal and was
239 consistent with the lack of Piezo1 within adhesions after transformation.

240 Although the measurements with the Cal-520 calcium sensor provided interesting insights into the
241 differences in spatial calcium signaling between normal and transformed cells, there remained several
242 specific questions about whether these calcium fluctuations were localized to sites of adhesion. The
243 diffusive nature of all Ca^{2+} dyes reduces the signal-to-noise ratio for calcium influx at sub-cellular locations,
244 providing only limited spatio-temporal information on local Ca^{2+} changes. In addition, under imaging
245 conditions sensitive to subcellular calcium events, Cal-520 had significant photo toxicity that caused rapid
246 increases in intracellular calcium levels limiting the observation window. To better quantify and understand

247 the details of calcium entry at the adhesions, we generated a novel focal adhesion targeted calcium sensor,
248 in which one of the latest most sensitive recombinant calcium sensors, jGCaMP7s, was linked to a paxillin
249 mScarlet-I construct (Figure 6A)[68]. This improved the signal-to-noise ratio specifically at the adhesions, and
250 the ratio between the calcium sensor and the mscarlet-I fluorescence enabled normalization of the calcium
251 levels based on the local sensor concentration.

252 When the paxillin calcium sensor was transfected in HFF, HT1080 and MDA-MB-231 cells, it localized
253 robustly to apparent adhesions. After overnight spreading, the intensity ratio of jGCaMP7s and mScarlet-I in
254 the focal adhesions of HFF cells showed frequent calcium spikes (Figure 6B,supplementary movie 7). The
255 calcium fluctuations were greatly reduced in Piezo1 knock down cells, indicating that Piezo1 was required for
256 the calcium fluctuations around the adhesions (Figure 6B-C,supplementary movie 8). Interestingly, in the
257 transformed HT1080 and MDA-MB-231 cells the calcium spikes at the adhesions were significantly weaker,
258 often there was no detectable calcium signal during a 1-hour observation window(Figure 6B,supplementary
259 movie 9-10). In the transformed cells, matrix adhesions still formed and disassembled, suggesting that
260 calcium entry around adhesions was not required for adhesion turnover in the transformed cells. These
261 results indicated that Piezo1 recruitment to adhesions in HFF cells enabled calcium spikes that could in turn
262 induce adhesion turnover; but in transformed cells, adhesion dynamics and cellular calcium fluctuations
263 were de-coupled.

264 *The central linker domain (1418-1656) of Piezo1 is required for Piezo1 adhesion*
265 *recruitment and alters cell morphology of non-transformed cells*

266 We proceeded to investigate potential molecular mechanisms of Piezo1 adhesion recruitment. So far, no
267 binding partners of Piezo1 at focal adhesions have been reported in the literature. The long lifetime of Piezo1
268 at the adhesions and the dependence of Piezo1 recruitment on actomyosin contractility led us to hypothesize
269 that Piezo1 bound to adhesion-linked components of the actin cytoskeleton stretched by cellular contractility.
270 Upon examining the 3D architecture of Piezo1(*47*), we identified a long intracellular linker as a potential
271 interaction site between Piezo1 and the actin cytoskeleton, as it has the most exposed intracellular region and

272 is in close proximity to the CTD and beam region that is critical for its force dependent activation (Figure
273 7A)(*48*).

274 This long intracellular linker region was largely unresolved in the Cryo-EM structures and connected the
275 beam to the clasp and via another unresolved loop to Piezo1 repeat B(*47*, *49*). Previous biophysical studies
276 showed that deletions at the proximal portion of the loop influenced the biophysical properties of the channel
277 via effects on the latch domain(*50*). However the distal end was not explored in those studies.

278 To check the potential function of the linker region of Piezo1, we first made a mNeongreen construct of the
279 larger region of human Piezo1 (residue 1418-1656;mNeonlinker) that contained the unstructured loop region,
280 the clasp and a second disordered loop previously shown to be able to house fluorescent tags(*38*). We next
281 checked for its localization and interaction with Piezo1. As shown in Figure 7B, the mNeonlinker construct
282 expressed in HFF cells appeared to be diffusely distributed with no apparent concentrations. However, Piezo1
283 recruitment to adhesions was reduced as was adhesion size with overexpression of the mNeonlinker (Figure
284 7B). This is consistent with the hypothesis that at high expression levels the mNeonlinker domain acted as a
285 dominant negative competitor and displaced Piezo1 from adhesions. When we checked the morphology of
286 the cells, HFF cells had significantly lower cell spread area and aspect ratio with the mNeonlinker over-
287 expression, which resembled the morphology change of HFF cells after Piezo1 knock-down (Figure 7B-C).
288 These results were consistent with the hypothesis that the recruitment of Piezo1 to focal adhesions in non-
289 transformed cells activated local calcium fluctuations in surrounding adhesions, and the calcium signal led to
290 adhesion maturation and cell polarization. In the case of transformed cells where Piezo1 did not localize to
291 adhesions, expression of mNeonlinker should have caused minimal effect on cell morphology. Indeed,
292 expression of mNeonlinker in HT1080 cells caused no change in morphology, cell spread area or aspect ratio
293 compared with controls (Figure 7B-C).

294 To further check if this linker region of Piezo1 indeed harboured focal adhesion binding sites, we generated
295 several Piezo1 mutants with the linker regions deleted (short: Piezo1 Δ1443-1556and long: Piezo1 Δ1443-
296 1473). The Δ1443-1473 deletion removed only residues from the oop region and the larger deletion Δ1443-

297 1556 removed much of the clasp domain. When we expressed these deletion mutants in FAK -/- MEF cells
298 that had prominment recruitment of WT Piezo1 to adhesions, we observed normal Piezo1 adhesion
299 recruitment of Piezo1 Δ1443-1473 mutant and diffusive Piezo1 localization of the Δ1443-1556 mutant (Figure
300 S7 and supplementary movie11-12). Electrophysiological characterization in Piezo1 KO HEK293T cells showed
301 that the Δ1443-1473 mutant had normal stretch induced channel activity while the Δ1443-1556 mutant was
302 not functional (Figure S8).

303 Taking these data together, it appeared that the linker domain (residues 1418-1656) and most likely the clasp
304 region of Piezo1 harbored a binding site for focal adhesion components that recruited Piezo1 to focal
305 adhesions in a force-dependent manner in non-transformed cells at the membrane-cytoplasm interface.

306 *Discussion*

307 In this study, we show that Piezo1 has important functions in focal adhesion dynamics in normal cells
308 but not in transformed cells. Normal fibroblasts, epithelial and endothelial cells form focal adhesions on
309 fibronectin where Piezo1 concentrates in a force-dependent process. The lifetime of Piezo1 in the adhesions
310 is similar to that of integrins and longer than typical adhesion proteins, which implies that it complexes
311 stably with adhesion bound proteins. Sustained contraction forces are needed for Piezo1 localization to
312 adhesions; and when contraction is inhibited, it could leave adhesions before the dissociation of adhesion
313 components such as integrin and talin. Piezo1 localization to focal adhesions leads to the dissociation of
314 integrin β3 containing adhesions but not integrin β1 adhesions on fibronectin. This localization is also lost in
315 transformed cells, including virus-transformed somatic cells (e.g. HEK293T) as well as tumor cell lines from
316 different tissues. When somatic cells are transformed such as in the case of TPM 2.1 knock down, the
317 recruitment of Piezo1 to adhesions is dramatically reduced similar to the transformed cancer lines tested.
318 Calcium levels in the vicinity of adhesions are higher and have many more local fluctuations in normal cells
319 compared with transformed cells. Binding to adhesions depends upon an unstructured cytoplasmic domain
320 of Piezo1 (aa 1418-1656). These findings indicate that Piezo1 has a number of complex interactions, which

321 depend upon contractility, the transformed state, as well as specific integrin-matrix interactions. Piezo1
322 appears to have multiple context-dependent functions in normal and transformed cells that need to be
323 analyzed temporally and spatially in a defined mechanical environment.

324 Piezo1 was first identified as an integrin-interacting protein which had a role in adhesion formation(*28*).
325 Our results reinforce those findings and further indicate that Piezo1 binds in a complex with integrins but
326 not with adhesion proteins such as talin or paxillin, which have much more rapid recovery rates after
327 photobleaching. Further, inhibition of PTPN12 activity or expression of the *Shigella* IpaA effector stabilizes
328 adhesion proteins even after inhibition of myosin but does not prevent Piezo1 dissociation. Piezo1's rapid
329 dissociation upon myosin inhibition is rapidly reversed upon washout of the myosin inhibitor. The rate of
330 return to the adhesions is much more rapid than during initial adhesion formation, indicating that the
331 recruitment of Piezo1 at adhesions may depend on a force-sensitive protein or activation of a force-
332 dependent enzyme that is retained at adhesion sites during myosin inhibition. Overexpression of a linker
333 region of human Piezo1 (aa 1418-1656) acts as a dominate negative, displacing Piezo1 from adhesions,
334 implying that this linker region of Piezo1 harbours the interacting site for adhesion binding. The lack of
335 adhesion maturation after depletion of Piezo1 strongly supports the hypothesis that Piezo1 has an important
336 role in the force-dependent maturation of adhesions on rigid surfaces, and this does not occur in
337 transformed cells.

338 Since the discovery of Piezo1's role as a mechanosensitive ion channel in eukaryotic cells, the regulation
339 mechanism of Piezo1's function in the various physiological activities of cells has been under heavy
340 investigation(*51*, *52*). The classical model of Piezo1's physiological function assumes that it is diffusive in the
341 plasma membrane and is activated locally through membrane bilayer tension or curvature changes that
342 occur through cytoskeletal-dependent mechanical events(*26*, *34*, *38*, *47*, *53*). Several recent studies have
343 clearly shown that the cystoskeletal environment influences Piezo1 function(*38*), including the observation
344 that Piezo1 localizes to the adhesions of some glioblastoma cell lines, which facilitates their growth and
345 invasion(*27*). The unusual nature of these glioblastoma lines indicates that they may be more like normal

346 cells than transformed cells (Yao et al unpublished results). In our study, we systematically examined
347 Piezo1's spatial distribution across many cell types from different tissues of origin and discovered that Piezo1
348 adhesion localization is much more prominent in non-transformed normal cells compared with transformed
349 cells such as most tumor cell lines. Binding to the adhesions in normal cells catalyzes adhesion maturation
350 and disassembly that correlates with cell growth.

351 Interestingly, in contrast to the reduced calcium transients that we observed in resting transformed
352 cells, we recently reported that mechanical perturbations, such as stretching or ultrasound treatment, cause
353 Piezo1-dependent increases in cytoplasmic Ca^{2+} levels and subsequent apoptosis of transformed but not
354 normal cells(*16*). These observations are difficult to explain in terms of fluctuations in either mechanical
355 forces on adhesions or membrane tension, especially since fewer Ca^{2+} fluctuation events are observed in
356 transformed cells whereas Ca^{2+} flickering events near adhesion sites are common in normal cells. With
357 regard to membrane tension, typical measurements of membrane tension in cells report values that are 2-3
358 orders of magnitude smaller than those needed to activate Piezo1 in vitro(*54*, *55*). Certainly, the pattern of
359 Ca^{2+} activation in the HFF cells in the vicinity of adhesions is consistent with previous results(*46*, *56*, *57*), but
360 it is not consistent with the simplistic model of very high membrane tension for the whole cell. Rather, there
361 appear to be local activation events that involve elements from the adhesions that may alter local
362 membrane tension/curvature or the association of membrane/cytoskeletal proteins that can modulate the
363 mechanical gating of Piezo1 activity(*53*, *58*, *59*). Although Piezo1 appears in many different mechanical
364 functions, the activation mechanism of Piezo1 is complex and both contributions from membrane tension
365 and interaction with cytoskeletal proteins may modulate its activity(*35*, *58*).

366 We recently showed that transformed cancer cells are depleted of the rigidity sensing, local contraction
367 units(*22*, *43*). There is a conserved set of cytoskeletal proteins that are able to assemble into local rigidity
368 sensing contractile structures in normal cells. After the depletion of any one of several cytoskeletal proteins
369 critical for rigidity sensing and contractile pair assembly, the cell will be transformed and will no longer sense
370 substrate rigidity. Transformation also involves changes in adhesion morphology and composition(*22*). The

371 differences in the adhesion components in normal and transformed cells that contribute to the adhesion
372 phenotype are still an open question but the mRNA levels of over 700 proteins are altered upon
373 transformation by tropomyosin 2.1 depletion[22]. An important function of the rigidity sensors is in the
374 maturation of focal adhesions that contain Piezo1 and without Piezo1 the mature adhesions do not form.
375 This further fits with the absence of any differences between transformed cell adhesions with and without
376 Piezo1. Thus, we suggest that normally both the maturation and the disassembly of focal adhesions is
377 catalyzed by Piezo1. In addition, whether the differences in Piezo1 recruitment in the transformed and
378 somatic cell lines are caused by changes in the molecular interactions or tension states of these cells remains
379 an open question and awaits further investigation.

380 Our model of the function of Piezo1 in Figure 8 emphasizes the catalytic role of Ca^{2+} entry in the life
381 cycle of the adhesions in normal cells. Initially, the nascent adhesions seed actin filament formation, myosin
382 bipolar filaments pull on the actin in the rigidity-sensing contractions, and there is a calcium-dependent
383 cleavage of talin1 that is needed for growth(*8*),[20]. If the matrix is rigid, then adhesions mature through
384 enzymatic modifications that trigger the maturation process. Components in the adhesions are stretched by
385 traction forces and then can bind Piezo1 which permits Ca^{2+} entry in a positive feedback cycle for the further
386 maturation of the adhesion. However, when the concentration of Piezo1 reaches a threshold, there is
387 excessive Ca^{2+} entry and recruitment of calpain that now hydrolyzes components of the adhesion, causing
388 the disassembly of the adhesion. The maturation process requires the rigidity sensing complex and will not
389 occur in transformed (cancer) cells. This model indicates that covalent modification of adhesion
390 components during maturation as well as traction forces on those components are necessary for Piezo1
391 binding. Further understanding of Piezo1 functions requires dynamic studies of Piezo1 at the appropriate
392 time and location during cell spreading or migration.

393 There is growing evidence that covalent modifications in maturing adhesions alter adhesion proteins as
394 well as possibly membrane proteins in normal cells(*20*, *60*). The release of Ca^{2+} near adhesions contributes to
395 protein processing by the adhesion signaling hub, which is needed for adhesion maturation and cell growth

396 on a rigid fibronectin matrix possibly through a localized calpain-dependent pathway. Our new paxillin-
397 associated calcium indicator shows that the Piezo1-dependent calcium transients are much more numerous
398 than observed with the cytoplasmic calcium indicator. Thus, the localization of Piezo1 to the adhesions
399 under force will provide a very localized activation of calpain and other calcium-dependent enzymes to
400 modify adhesions and membrane proteins in specific locations. Besides Piezo1, other membrane channels
401 such as TRPV4, Orai, L-type channels, TRPM4 and TRPM7 have been implicated in the regulation of adhesion
402 morphology, dynamics and cell migration(*20*, *23*, *61*, *62*). The non-interchangable role of these channels
403 suggests that there might exist coopertivity between these channels, such as calcium-dependent calcium
404 release (*63*).

405 In transformed cells, growth appears independent of local Ca^{2+} entry at rigid matrix sites and Piezo1 is
406 decoupled from traction forces and adhesion signaling. It is commonly believed that transformed cells are
407 related to wound healing where cell growth for repair is needed and localized signaling from matrices is not
408 needed(*64*) . Further, in many cancers, the elevated growth rates correlate with high levels of calpain that
409 could amplify small Ca^{2+} leaks to support the growth activity. This could help to explain how stretch could
410 cause general changes in the plasma membrane activating Ca^{2+} entry through Piezo1 by local membrane
411 tension or curvature changes that would cascade into an apoptotic process[16]. Most importantly, the general
412 activation of growth in cancer cells appears to occur without localized signaling at adhesions by Piezo1.

413 In the larger picture of adhesion maturation, there are many adhesion proteins that bind to adhesions in
414 a force-dependent manner(*65*, *66*). It is surprising, however, that the inhibition of the release of many
415 adhesion proteins by the inhibition of PTPN12 or expression of virulence bacterial protein IpaA did not block
416 the release of Piezo1 upon myosin inhibition. Further, Piezo1 is strongly bound to the adhesions and has a
417 lifetime similar to integrin β3 in adhesions that depends on contractility. The stronger retention of Piezo1 at
418 adhesions upon the transition from integrin β3 to β1 may aid in the stabilization of such adhesions for
419 development of higher forces on matrix contacts through continued local influx of calcium(*67*). The integrin
420 subtype dependence of Piezo1 dynamics could be of great importance for the physiological function of

421 Piezo1, e.g. in vascular development(*4*). Piezo1 knock-out mice die as embryos due to vascular defects, and
422 inactivation of β3 inhibits the angiogenesis process. Mechanical forces such as shear forces are very
423 important in these processes(*4*). The force dependent co-localization and turnover of Piezo1 at β3 integrin
424 adhesions could be synergistic with downstream events and provides a mechanism of tension-dependent
425 vascular growth that is critical in development. Thus, we suggest that the contractility dependent
426 recruitment of Piezo1 to focal adhesions is a novel crosstalk mechanism between the two major
427 mechanotrasduction hubs of the cell that play critical roles in adhesion function which are lost in most
428 tumor cells (Figure 8) .

429 *Material and methods*

430 *Cell culture and constructs:*

431 The mEmerald-integrin β3, mEmerald-integrin β1, paxillin-mapple, paxillin-BFP and talin-GFP were gifts
432 from Michael Davidson (Addgene plasmid # 56330, #54129, #54935). The piezo1-GFP-1591 and piezo1-
433 mruby3-1591 plasmids were generated as previously described(*38*). The RhoAV14 construct was from
434 Schwartz lab(*68*). TPM2.1-YFP construct was from Gunning Lab(*69*). The A431 ipa peptide plasmid was
435 generated as previously described(*70*). The paxillin calcium sensor was generated by PCR cloning of
436 jGCaMP7s segment from pGP-CMV-jGCaMP7s plasmid from addgene(*71*) and inserted into the N-terminal of
437 a paxillin-mScarleti construct derived from paxillin-mapple.

438 siRNA for tropomyosin 2.1 was synthesized as previously described by Dharmacon(*43*). siRNA for human
439 Piezo1 was ordered from Dharmacon (ON-TARGETplus human Piezo1 siRNA, SMARTpool, L-020870-03-0010)
440 and Merck Sigma-Aldrich (SASI_HS01_00208585) or Life Technologies(cat no #21816). RT-PCR analysis
441 showed that both siRNA caused >90% knock down at the mRNA level two days after transfection. The siRNA
442 were transfected using RNAiMAX reagent from ThermoFisher following manufacture's protocols.

443 Human Foreskin fibroblast (HFF), HUMEC, HUVEC, HT1080, A2058, A375P, and MCF-10A cells were
444 obtained from ATCC. MDA-MB-231, SKOV3, cells were from Ruby Huang's lab. HEK293T cells with piezo1 KO
445 were from Ardem Patapoutian's lab. HFF, MDA-MB-231, HEK293T Piezo1 KO and cells were cultured in 1X
446 DMEM supplemented with 5 mM sodium pyruvate and 10% of Hi-FBS. MCF-10A cells were cultured using
447 fomulated media as reported previously(*22*) and HUVEC cells were cultured in endothelial growth media
448 from Sigma.

449 ## Ca^{2+} *influx measurements*

450 For calcium level measurements using force sensors, cells were transfected with the GCAMP7S-paxillin-
451 mScarleti construct and seeded on fibronectin coated glass bottom coverslips overnight. Transfected cells
452 were imaged using TirfM microscrope using 488 and 561 laser lines. Specific band pass excitation/emission
453 filter cubes (GFP-HQ and mCherry-HQ from Nikon) were used to avoid fluorescence crosstalk between
454 channels. For comparison between different samples, all imaging parameters (laser power, tirf angle,
455 camera exposures) were kept constant. Only cells with comparable calcium sensor expression levels (judging
456 from fluorescence intensity from mScarlet channel) were picked for analysis to minimize potential bias due
457 to sensor concentration differences.

458 The local Ca^{2+} influx of the cells was measured following Ellefsen et. al(*26*). Briefly, the HFF cells were
459 loaded with 4 uM Ca^{2+} indicator Cal-520-AM for 2 hours. Then the cells were detached using enzyme free
460 dissociation media and resuspended in complete growth media. The cells were allowed to recover in
461 suspension for 20 min before seeding on glass bottom coverslips coated with fibronectin. After 2 hours the
462 buffer was switched to Ringer's balanced salt and proceeded for imaging on Nikon Tirf system with pulsed
463 laser lines to minimize photodamage of the sample(*72*). The calcium images of individuals cells were
464 acquired at 100Hz for 5000 frames. The deltaF/F images of the cells were generated using a custom matlab
465 script to reveal individual Ca^{2+} influx events. Such events were tracked using the Trackmate ImageJ
466 plugin(*73*).

467 ## *Cell spreading assay*

468 In the cell spreading assay, cells were transfected with respective plasmids 36-48 hours before
469 experiments using Neon transfection system (Thermo Fisher) or JetOptimus chemical transfection reagent
470 (PolyPlus) following manufacturer's recommendations. On the day of experiment, the cells were detached
471 using an enzyme-free cell detaching buffer (Cell Dissociation Buffer, enzyme-free, PBS, Gibco), spun-down
472 and resuspended in complete media (1X DMEM, 10% FBS). The suspended cells were allowed to recover by
473 incubating in the cell culture hood for 20 min and then seeded onto glass bottom Petri dishes coated with
474 ECM molecules of interest (10 ug/ml collagen I, 10 ug/ml fibronectin, 10 ug/ml VTN-N, and 10 ug/ml laminin
475 for 1 hour). Imaging was done on a Nikon Tirf system with 405,488,561 and 640 laser lines. The cell
476 spreading area and adhesion size were analyzed automatically using CellProfiler(*74*).

477 ## *Immunostaining and antibodies*

478 Cells of interest seeded on glass bottom Petri dishes were fixed with 4% paraformaldehyde (PFA) for 30
479 min at 37 degrees and washed with 1X PBS three times. The fixed cells were permeabilized/blocked by
480 incubation with TBST (1X TBS, 0.1% Tween-20) containing 5% Bovine Serum Abumin (BSA) overnight at 4
481 degrees. Primary antibodies were diluted in TBST, 5% BSA solution according to manufactures'
482 recommendations and added to the cells overnight at 4 degrees. The stained cells were washed with 1X PBS
483 and stained with secondary antibody for 1 hour at room temperature.

484 Polyclonal Rabbit and monoclonal mouse anti-Piezo1 was from Novus Biologicals (NBP1-78446, NBP2-
485 75617), both have been validated by Piezo1 knock down/knock off experiments(*15*, *75*). For all Piezo1
486 localization quantifications, the monoclonal NBP2-75617 antibody was used. Mouse anti-Paxillin antibody
487 was from Merck Millipore (MAB 3060), Rabbit anti-paxillin antibody was from abcam(ab32115). Mouse anti-
488 activated integrin β1 antibody was from BD Biosciences (9EG7). Rat anti integrin αvβ3 was from
489 Millipore(LM609).

490 ## *FRAP analysis*

491 FRAP analyses were carried out on an ILAS2 TIRF image system similar to reported previously. Briefly,
492 HFF, HT1080, or MDA-MB-231 cells transiently co-transfected with Piezo1-GFP and Paxillin-mapple, or
493 Piezo1-mruby3 and mEmerald-integrin β3 were seeded on Fibronectin coated glass bottom dishes overnight.
494 2-5 square-shaped regions of interests (~3 um length) covering focal adhesions were selected for each cell
495 and bleached. The recovery of fluorescence in both fluorescent channels was observed for from 360 to 600
496 seconds after photobleaching. The recovery curves were normalized by dividing by average intensity of each
497 ROI before bleaching and the average and standard deviation of the recovery were calculated.

498 *Electrophysiology of the Pieoz1 linker mutants*

499 Piezo1 KO HEK293T cells were plated on 35 mm dishes and transfected with lipofectamine 3000 as per
500 the manufacturers instructions 48 h prior to patch-clamp analysis. The extracellular solution for cell-attached
501 patches contained high K^+ to zero the membrane potential; it consisted of 90 mM potassium aspartate, 50
502 mM KCl, 1 mM $MgCl_2$ and 10 mM HEPES (pH 7.2) adjusted with 5 M KOH. The pipette solution contained 140
503 mM NaCl, 3 mM KCl, 1 mM MgCl2, 1 mM CaCl2 with 10 mM HEPES (pH 7.2) adjusted with sodium hydroxide.
504 Negative pressure was applied to patch pipettes using a High-Speed Pressure Clamp-1 (ALA Scientific
505 Instruments, Farmingdale, NY, USA) and recorded in millimetres of mercury (mmHg) using a piezoelectric
506 pressure transducer (WPI, Sarasota, FL, USA). Borosilicate glass pipettes (Sigma-Aldrich) were pulled with a
507 vertical pipette puller (PP-83, Narashige, Tokyo, Japan) to produce electrodes with a resistance of ~2 MΩ.
508 The Piezo1 currents were amplified using an AxoPatch 200B amplifier (Axon Instruments, Union City, CA,
509 USA), and data were sampled at a rate of 10 kHz with 1 kHz filtration and analysed using pCLAMP10
510 software (Axon Instruments).

511 *Acknoledgements*

512 We would like to thank Professor Alexander Beshardsky and Dr Benjamin T. Goult for critical discussions and
513 the microscopy core and protein cloning expression core facility of Mechanobiology Institute for their
514 technical support.

Author Contributions:

M.Y, C.C and M.S designed research, M.Y, C. C, A.J, D.C, JV. L and A.H performed experiments and analyzed the data. M.Y, C.C and G. TVN contributed to new reagents/methods. M.S and B.M supervised the research. M.Y, C.C and M.S wrote the paper.

Conflict of Interest :

The authors declare no conflict of interest.

References

1. B. Geiger, J. P. Spatz, A. D. Bershadsky, Environmental sensing through focal adhesions. *Nat. Rev. Mol. Cell Biol.* **10**, 21–33 (2009).

2. V. Vogel, M. Sheetz, Local force and geometry sensing regulate cell functions. *Nat. Rev. Mol. Cell Biol.* **7**, 265–75 (2006).

3. R. K. Jain, J. D. Martin, T. Stylianopoulos, The Role of Mechanical Forces in Tumor Growth and Therapy. *Annu. Rev. Biomed. Eng.* **16**, 321–346 (2014).

4. J. Li, B. Hou, S. Tumova, K. Muraki, A. Bruns, M. J. Ludlow, A. Sedo, A. J. Hyman, L. McKeown, R. S. Young, N. Y. Yuldasheva, Y. Majeed, L. A. Wilson, B. Rode, M. A. Bailey, H. R. Kim, Z. Fu, D. A. L. L. Carter, J. Bilton, H. Imrie, P. Ajuh, T. N. Dear, R. M. Cubbon, M. T. Kearney, K. R. Prasad, P. C. Evans, J. F. X. X. Ainscough, D. J. Beech, Piezo1 integration of vascular architecture with physiological force. *Nature*. **515**, 279–282 (2014).

5. A. D. Bershadsky, N. Q. Balaban, B. Geiger, Adhesion-dependent cell mechanosensitivity. *Annu. Rev. Cell Dev. Biol.* **19**, 677–95 (2003).

535 6. T. Panciera, L. Azzolin, M. Cordenonsi, S. Piccolo, Mechanobiology of YAP and TAZ in physiology and
536 disease. *Nat. Rev. Mol. Cell Biol.* (2017), doi:10.1038/nrm.2017.87.

537 7. B. Trappmann, J. E. Gautrot, J. T. Connelly, D. G. T. Strange, Y. Li, M. L. Oyen, M. A. Cohen Stuart, H.
538 Boehm, B. Li, V. Vogel, J. P. Spatz, F. M. Watt, W. T. S. Huck, Extracellular-matrix tethering regulates
539 stem-cell fate. *Nat. Mater.* **11**, 642–649 (2012).

540 8. H. Wolfenson, B. Yang, M. P. Sheetz, Steps in Mechanotransduction Pathways that Control Cell
541 Morphology. *Annu. Rev. Physiol.* **81**, 585–605 (2019).

542 9. E. R. Horton, A. Byron, J. A. Askari, D. H. J. Ng, A. Millon-Frémillon, J. Robertson, E. J. Koper, N. R. Paul,
543 S. Warwood, D. Knight, J. D. Humphries, M. J. Humphries, Definition of a consensus integrin
544 adhesome and its dynamics during adhesion complex assembly and disassembly. *Nat. Cell Biol.* **17**,
545 1577–1587 (2015).

546 10. A. del Rio, R. Perez-Jimenez, R. Liu, P. Roca-Cusachs, J. M. Fernandez, M. P. Sheetz, Stretching single
547 talin rod molecules activates vinculin binding. *Science (80-.).* **323**, 638–41 (2009).

548 11. M. Yao, B. T. Goult, B. Klapholz, X. Hu, C. P. Toseland, Y. Guo, P. Cong, M. P. Sheetz, J. Yan, The
549 mechanical response of talin. *Nat. Commun.* **7**, 11966 (2016).

550 12. B. Yang, Z. Z. Lieu, H. Wolfenson, F. M. Hameed, A. D. Bershadsky, M. P. Sheetz, *Nano Lett.*, in press,
551 doi:10.1021/acs.nanolett.6b02995.

552 13. W. H. Goldmann, Role of vinculin in cellular mechanotransduction. *Cell Biol. Int.* **40**, 241–256 (2016).

553 14. E. Bates, Ion Channels in Development and Cancer. *Annu. Rev. Cell Dev. Biol.* **31**, 231–247 (2015).

554 15. S. A. Gudipaty, J. Lindblom, P. D. Loftus, M. J. Redd, K. Edes, C. F. Davey, V. Krishnegowda, J.
555 Rosenblatt, Mechanical stretch triggers rapid epithelial cell division through Piezo1. *Nature*. **543**,
556 118–121 (2017).

557 16. A. Tijore, M. Yao, Y. H. Wang, A. Hariharan, Y. Nematbakhsh, B. Lee Doss, C. T. Lim, M. Sheetz, B. Lee,
558 C. Teck, M. Sheetz, Biomaterials Selective killing of transformed cells by mechanical stretch.
559 *Biomaterials*. **275**, 120866 (2021).

560 17. A. Bhatt, I. Kaverina, C. Otey, A. Huttenlocher, Regulation of focal complex composition and
561 disassembly by the calcium-dependent protease calpain. *J. Cell Sci.* **115**, 3415–25 (2002).

562 18. S. J. Franco, M. a Rodgers, B. J. Perrin, J. Han, D. a Bennin, D. R. Critchley, A. Huttenlocher, Calpain-
563 mediated proteolysis of talin regulates adhesion dynamics. *Nat. Cell Biol.* **6**, 977–83 (2004).

564 19. S. J. Franco, Regulating cell migration: calpains make the cut. *J. Cell Sci.* **118**, 3829–3838 (2005).

565 20. M. Saxena, R. Changede, J. Hone, H. Wolfenson, M. P. Sheetz, Force-Induced Calpain Cleavage of Talin
566 Is Critical for Growth, Adhesion Development, and Rigidity Sensing. *Nano Lett.* **17**, 7242–7251 (2017).

567 21. T. Travers, H. Shao, B. a Joughin, D. a Lauffenburger, A. Wells, C. J. Camacho, Tandem
568 phosphorylation within an intrinsically disordered region regulates ACTN4 function. *Sci. Signal.* **8**,
569 ra51 (2015).

570 22. B. Yang, H. Wolfenson, V. Y. Chung, N. Nakazawa, S. Liu, J. Hu, R. Y. J. Huang, M. P. Sheetz, Stopping
571 transformed cancer cell growth by rigidity sensing. *Nat. Mater.* **19**, 239–250 (2020).

572 23. S. Yang, J. J. Zhang, X. Y. Huang, Orai1 and STIM1 Are Critical for Breast Tumor Cell Migration and
573 Metastasis. *Cancer Cell*. **15**, 124–134 (2009).

574 24. K. Clark, M. Langeslag, B. van Leeuwen, L. Ran, A. G. Ryazanov, C. G. Figdor, W. H. Moolenaar, K.
575 Jalink, F. N. van Leeuwen, TRPM7, a novel regulator of actomyosin contractility and cell adhesion.
576 *EMBO J.* **25**, 290–301 (2006).

577 25. C. Wei, X. Wang, M. Chen, K. Ouyang, L.-S. Song, H. Cheng, Calcium flickers steer cell migration.
578 *Nature*. **457**, 901–905 (2009).

579 26. K. L. Ellefsen, J. R. Holt, A. C. Chang, J. L. Nourse, J. Arulmoli, A. H. Mekhdjian, H. Abuwarda, F.
580 Tombola, L. A. Flanagan, A. R. Dunn, I. Parker, M. M. Pathak, Myosin-II mediated traction forces
581 evoke localized Piezo1-dependent Ca2+ flickers. *Commun. Biol.* **2**, 298 (2019).

582 27. X. Chen, S. Wanggou, A. Bodalia, M. Zhu, W. Dong, J. J. Fan, W. C. Yin, H. K. Min, M. Hu, D. Draghici,
583 W. Dou, F. Li, F. J. Coutinho, H. Whetstone, M. M. Kushida, P. B. Dirks, Y. Song, C. chung Hui, Y. Sun, L.
584 Y. Wang, X. Li, X. Huang, A Feedforward Mechanism Mediated by Mechanosensitive Ion Channel
585 PIEZO1 and Tissue Mechanics Promotes Glioma Aggression. *Neuron*. **100**, 799-815.e7 (2018).

586 28. B. J. McHugh, R. Buttery, Y. Lad, S. Banks, C. Haslett, T. Sethi, Integrin activation by Fam38A uses a
587 novel mechanism of R-Ras targeting to the endoplasmic reticulum. *J. Cell Sci.* **123**, 51–61 (2010).

588 29. B. Coste, J. Mathur, M. Schmidt, T. J. Earley, S. Ranade, M. J. Petrus, A. E. Dubin, A. Patapoutian,
589 Piezo1 and Piezo2 Are Essential Components of Distinct Mechanically Activated Cation Channels.
590 *Science (80-.).* **330**, 55–60 (2010).

591 30. M. M. Pathak, J. L. Nourse, T. Tran, J. Hwe, J. Arulmoli, D. T. T. Le, E. Bernardis, L. A. Flanagan, F.
592 Tombola, Stretch-activated ion channel Piezo1 directs lineage choice in human neural stem cells.
593 *Proc. Natl. Acad. Sci.* **111**, 16148–16153 (2014).

594 31. C. Li, S. Rezania, S. Kammerer, A. Sokolowski, T. Devaney, A. Gorischek, S. Jahn, H. Hackl, K.
595 Groschner, C. Windpassinger, E. Malle, T. Bauernhofer, W. Schreibmayer, Piezo1 forms
596 mechanosensitive ion channels in the human MCF-7 breast cancer cell line. *Sci. Rep.* **5**, 1–9 (2015).

597 32. A. G. Solis, P. Bielecki, H. R. Steach, L. Sharma, C. C. D. Harman, S. Yun, M. R. de Zoete, J. N. Warnock,
598 S. D. F. To, A. G. York, M. Mack, M. A. Schwartz, C. S. Dela Cruz, N. W. Palm, R. Jackson, richard A.
599 Flavell, Mechanosensation of cyclical force by PIEZO1 is essential for innate immunity. *Nature*. **573**,
600 69–74 (2019).

601 33. I. Borbiro, D. Badheka, T. Rohacs, Activation of TRPV1 channels inhibits mechanosensitive piezo
602 channel activity by depleting membrane phosphoinositides. *Sci. Signal.* **8** (2015),
603 doi:10.1126/scisignal.2005667.

604 34. J. L. Nourse, M. M. Pathak, How cells channel their stress: Interplay between Piezo1 and the
605 cytoskeleton. *Semin. Cell Dev. Biol.* **71**, 3–12 (2017).

606 35. N. Bavi, J. Richardson, C. Heu, B. Martinac, K. Poole, PIEZO1-Mediated Currents Are Modulated by
607 Substrate Mechanics. *ACS Nano*. **13**, 13545–13559 (2019).

608 36. B. M. Gaub, D. J. Müller, Mechanical Stimulation of Piezo1 Receptors Depends on Extracellular Matrix
609 Proteins and Directionality of Force. *Nano Lett.* **17**, 2064–2072 (2017).

610 37. J. Albarrán-Juárez, A. Iring, S. Wang, S. Joseph, M. Grimm, B. Strilic, N. Wettschureck, T. F. Althoff, S.
611 Offermanns, Piezo1 and G q /G 11 promote endothelial inflammation depending on flow pattern and
612 integrin activation. *J. Exp. Med.* **215**, 2655–2672 (2018).

613 38. C. D. Cox, C. Bae, L. Ziegler, S. Hartley, V. Nikolova-Krstevski, P. R. Rohde, C. A. Ng, F. Sachs, P. A.
614 Gottlieb, B. Martinac, Removal of the mechanoprotective influence of the cytoskeleton reveals
615 PIEZO1 is gated by bilayer tension. *Nat. Commun.* **7**, 1–13 (2016).

616 39. H. Park, C. Valencia-Gallardo, A. Sharff, G. Tran Van Nhieu, T. Izard, Novel vinculin binding site of the
617 IpaA invasin of Shigella. *J. Biol. Chem.* **286**, 23214–21 (2011).

618 40. C. Valencia-Gallardo, D.-I. Aguilar-Salvador, H. Khakzad, C. Bou-Nader, C. Malosse, D. B. Lima, C. Bello,
619 B. Cocom-Chan, N. Quenech'Du, B. Mazhar, D. Javelaud, J. Fattaccioli, A. Mauviel, M. Fontecave, A.
620 Asnacios, J. Chamot-Rooke, L. Malmström, G. Tran Van Nhieu, Vinculin targeting by Shigella IpaA
621 promotes stable cell adhesion independent of mechanotransduction. *bioRxiv* (2019),
622 doi:10.1101/773283.

623 41. A. N. Tullio, D. Accili, V. J. Ferrans, Z. X. Yu, K. Takeda, A. Grinberg, H. Westphal, Y. A. Preston, R. S.
624 Adelstein, Nonmuscle myosin II-B is required for normal development of the mouse heart. *Proc. Natl.*
625 *Acad. Sci. U. S. A.* **94**, 12407–12412 (1997).

626 42. A. Elosegui-Artola, E. Bazellières, M. D. Allen, I. Andreu, R. Oria, R. Sunyer, J. J. Gomm, J. F. Marshall, J.
627 L. Jones, X. Trepat, P. Roca-Cusachs, Rigidity sensing and adaptation through regulation of integrin
628 types. *Nat. Mater.* **13**, 631–7 (2014).

629 43. H. Wolfenson, G. Meacci, S. Liu, M. R. Stachowiak, T. Iskratsch, S. Ghassemi, P. Roca-Cusachs, B.
630 O'Shaughnessy, J. Hone, M. P. Sheetz, B. O'Shaughnessy, J. Hone, M. P. Sheetz, Tropomyosin controls
631 sarcomere-like contractions for rigidity sensing and suppressing growth on soft matrices. *Nat. Cell*
632 *Biol.* **18**, 33–42 (2015).

633 44. J. Robertson, G. Jacquemet, A. Byron, M. C. Jones, S. Warwood, J. N. Selley, D. Knight, J. D.
634 Humphries, M. J. Humphries, Defining the phospho-adhesome through the phosphoproteomic
635 analysis of integrin signalling. *Nat. Commun.* **6**, 6265 (2015).

636 45. A. Byron, J. A. Askari, J. D. Humphries, G. Jacquemet, E. J. Koper, S. Warwood, C. K. Choi, M. J. Stroud,
637 C. S. Chen, D. Knight, M. J. Humphries, A proteomic approach reveals integrin activation state-
638 dependent control of microtubule cortical targeting. *Nat. Commun.* **6**, 6135 (2015).

639 46. G. Giannone, P. Rondé, M. Gaire, J. Beaudouin, J. Haiech, J. Ellenberg, K. Takeda, Calcium rises locally
640 trigger focal adhesion disassembly and enhance residency of focal adhesion kinase at focal adhesions.
641 *J. Biol. Chem.* **279**, 28715–28723 (2004).

642 47. Y. R. Guo, R. MacKinnon, Structure-based membrane dome mechanism for piezo mechanosensitivity.
643 *Elife*. **6**, 1–19 (2017).

644 48. Q. Zhao, H. Zhou, S. Chi, Y. Wang, J. Wang, J. Geng, K. Wu, W. Liu, T. Zhang, M. Q. Dong, J. Wang, X. Li,
645 B. Xiao, Structure and mechanogating mechanism of the Piezo1 channel. *Nature*. **554**, 487–492
646 (2018).

647 49. K. Saotome, S. E. Murthy, J. M. Kefauver, T. Whitwam, A. Patapoutian, A. B. Ward, Structure of the
648 mechanically activated ion channel Piezo1. *Nature*. **554**, 481–486 (2018).

649 50. J. Geng, W. Liu, H. Zhou, T. Zhang, L. Wang, M. Zhang, Y. Li, B. Shen, X. Li, B. Xiao, A Plug-and-Latch
650 Mechanism for Gating the Mechanosensitive Piezo Channel. *Neuron*. **106**, 438-451.e6 (2020).

651 51. J. Wu, A. H. Lewis, J. Grandl, Touch, Tension, and Transduction – The Function and Regulation of Piezo
652 Ion Channels. *Trends Biochem. Sci.* **42**, 57–71 (2017).

653 52. S. E. Murthy, A. E. Dubin, A. Patapoutian, Piezos thrive under pressure: Mechanically activated ion
654 channels in health and disease. *Nat. Rev. Mol. Cell Biol.* **18**, 771–783 (2017).

655 53. Y.-C. Lin, Y. R. Guo, A. Miyagi, J. Levring, R. MacKinnon, S. Scheuring, Force-induced conformational
656 changes in PIEZO1. *Nature* (2019), doi:10.1038/s41586-019-1499-2.

657 54. J. Dai, M. P. Sheetz, Membrane tether formation from blebbing cells. *Biophys. J.* **77**, 3363–3370
658 (1999).

659 55. R. Syeda, M. N. Florendo, C. D. Cox, J. M. Kefauver, J. S. Santos, B. Martinac, A. Patapoutian, Piezo1
660 Channels Are Inherently Mechanosensitive. *Cell Rep.* **17**, 1739–1746 (2016).

661 56. G. Giannone, P. Rondé, M. Gaire, J. Haiech, K. Takeda, Calcium oscillations trigger focal adhesion
662 disassembly in human U87 astrocytoma cells. *J. Biol. Chem.* **277**, 26364–26371 (2002).

663 57. S. Sen, S. Kumar, Combining mechanical and optical approaches to dissect cellular mechanobiology. *J.*
664 *Biomech.* **43**, 45–54 (2010).

665 58. C. D. Cox, N. Bavi, B. Martinac, Biophysical Principles of Ion-Channel-Mediated Mechanosensory
666 Transduction. *Cell Rep.* **29**, 1–12 (2019).

667 59. Z. Shi, Z. T. Graber, T. Baumgart, H. A. Stone, A. E. Cohen, Cell Membranes Resist Flow. *Cell*. **175**,
668 1769-1779.e13 (2018).

669 60. A. Schwartz[1], C. Hall[1], L. Barney[1], C. Babbitt[2], S. Peyton[1], Mechanosensing of Integrin α 6 and EGFR
670 Converges at Calpain 2 (2017), doi:10.1101/164525.

671 61. C. L. Yankaskas, K. Bera, K. Stoletov, S. A. Serra, J. Carrillo-garcia, S. Tuntithavornwat, P. Mistriotis, J.
672 D. Lewis, M. A. Valverde, K. Konstantopoulos, The fluid shear stress sensor TRPM7 regulates tumor
673 cell intravasation (2021).

674 62. A. K. Efremov, M. Yao, Y. Sun, Y. H. Tee, M. P. Sheetz, A. D. Bershadsky, B. Martinac, J. Yan,
675 Application of piconewton forces to individual filopodia reveals mechanosensory role of L-type Ca2+
676 channels. *Biomaterials*. **284**, 121477 (2022).

677 63. C. L. Gilchrist, H. A. Leddy, L. Kaye, N. D. Case, K. E. Rothenberg, D. Little, W. Liedtke, B. D. Hoffman, F.
678 Guilak, TRPV4-mediated calcium signaling in mesenchymal stem cells regulates aligned collagen
679 matrix formation and vinculin tension. *Proc. Natl. Acad. Sci. U. S. A.* **116**, 1992–1997 (2019).

680 64. M. Sheetz, *Annu. Rev. Cell Dev. Biol.*, in press, doi:10.1146/annurev-cellbio-100818-125227.

681 65. S. W. Moore, P. Roca-Cusachs, M. P. Sheetz, Stretchy proteins on stretchy substrates: the important
682 elements of integrin-mediated rigidity sensing. *Dev. Cell*. **19**, 194–206 (2010).

683 66. C. G. Galbraith, K. M. Yamada, M. P. Sheetz, The relationship between force and focal complex
684 development. *J. Cell Biol.* **159**, 695–705 (2002).

685 67. P. Roca-Cusachs, A. del Rio, E. Puklin-Faucher, N. C. Gauthier, N. Biais, M. P. Sheetz, Integrin-
686 dependent force transmission to the extracellular matrix by -actinin triggers adhesion maturation.
687 *Proc. Natl. Acad. Sci.* **110**, E1361–E1370 (2013).

688 68. X. D. Ren, W. B. Kiosses, M. A. Schwartz, Regulation of the small GTP-binding protein Rho by cell
689 adhesion and the cytoskeleton. *EMBO J.* **18**, 578–585 (1999).

690 69. G. Gateva, E. Kremneva, T. Reindl, T. Kotila, K. Kogan, L. Gressin, P. W. Gunning, D. J. Manstein, A.
691 Michelot, P. Lappalainen, Tropomyosin Isoforms Specify Functionally Distinct Actin Filament
692 Populations In Vitro. *Curr. Biol.* **27**, 705–713 (2017).

693 70. C. Valencia-Gallardo, C. Bou-Nader, D. Aguilar, N. Carayol, N. Quenech'Du, L. Pecqueur, H. Park, M.
694 Fontecave, T. Izard, G. T. Van Nhieu, Cell adhesion promoted by a unique Shigella IpaA vinculin- and
695 talin-binding site. *bioRxiv*, 329136 (2018).

696 71. H. Dana, Y. Sun, B. Mohar, B. K. Hulse, A. M. Kerlin, J. P. Hasseman, G. Tsegaye, A. Tsang, A. Wong, R.
697 Patel, J. J. Macklin, Y. Chen, A. Konnerth, V. Jayaraman, L. L. Looger, E. R. Schreiter, K. Svoboda, D. S.
698 Kim, High-performance calcium sensors for imaging activity in neuronal populations and
699 microcompartments. *Nat. Methods*. **16**, 649–657 (2019).

700 72. G. Donnert, C. Eggeling, S. W. Hell, Major signal increase in fluorescence microscopy through dark-
701 state relaxation. *Nat. Methods*. **4**, 81–86 (2007).

702 73. J. Y. Tinevez, N. Perry, J. Schindelin, G. M. Hoopes, G. D. Reynolds, E. Laplantine, S. Y. Bednarek, S. L.
703 Shorte, K. W. Eliceiri, TrackMate: An open and extensible platform for single-particle tracking.
704 *Methods*. **115**, 80–90 (2017).

705 74. C. McQuin, A. Goodman, V. Chernyshev, L. Kamentsky, B. A. Cimini, K. W. Karhohs, M. Doan, L. Ding,
706 S. M. Rafelski, D. Thirstrup, W. Wiegraebe, S. Singh, T. Becker, J. C. Caicedo, A. E. Carpenter,
707 CellProfiler 3.0: Next-generation image processing for biology. *PLoS Biol.* **16**, e2005970 (2018).

75. J. V. Li, C.-A. Ng, D. Cheng, Z. Zhou, M. Yao, Y. Guo, Z.-Y. Yu, Y. Ramaswamy, L. A. Ju, P. W. Kuchel, M. P. Feneley, D. Fatkin, C. D. Cox, Modified N-linked glycosylation status predicts trafficking defective human Piezo1 channel mutations. *Commun. Biol.* **4**, 1038 (2021).

712 *Figures:*

713 Figure 1

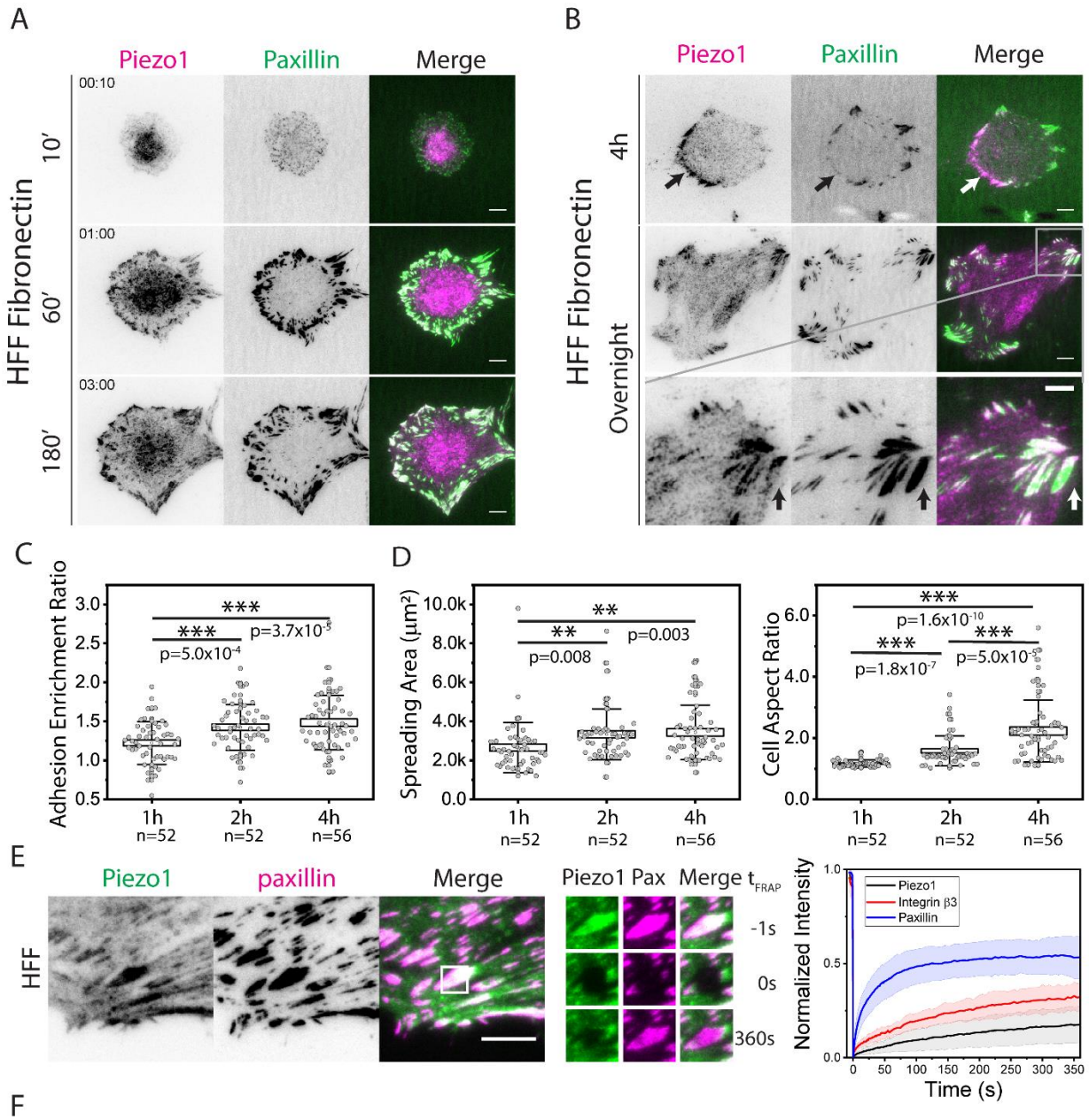

Piezo1 (n=18)		Integrin β3 (n=7)		Paxillin (n=11)	
Mobile Fraction	τ (s)	Mobile Fraction	τ (s)	Mobile Fraction	τ (s)
0.09 [0.07,0.11]	118.0 [104.6,131.3]	0.36 [0.27,0.46]	92.9 [69.4,116.4]	0.60 [0.53,0.66]	25.4 [15.3,35.6]

714

715 **Figure 1. Piezo1 is stably recruited to maturing adhesions on fibronectin surfaces.** (A)Time lapse of cell

716 spreading of HFF cells seeded on fibronectin coated glass surface. The cells are transiently expressing Piezo1-

717 mruby3 and paxillin-BFP. Scale Bars denote 10 um. (B) Localization of Piezo1 spreading on fibronectin
718 surface during polarization and in stable condition. Scale Bars denote 10 um in the main figure and 5um in
719 the zoom. (C) Adhesion enrichment of Piezo1 at 1h, 2h and 4h after cell seeding. The adhesion enrichment
720 was defined as the average intesity ratio of Piezo1 in the adhesions and background. (D) Cell spreading area
721 and aspect ratio 1h, 2h and 4h after cell seeding. The significance were calculated using two sample t-test.
722 (E) Left panel: Live TIRF images of Human Foreskin Fibroblast (HFF) cells transiently transfected with Piezo1-
723 GFP and paxillin-mapple on fibronectin coated surfaces. The adhesion region marked by white square was
724 bleached and snapshots of fluorescent recovery for Piezo1 and talin are shown in the zoom in figure on
725 bottom. Scale Bars denote 5 um. Right panel: The FRAP recovery curve of the bleached region (mean $\pm$ std).
726 (F) The fitted mobile fraction and recovery rates from the FRAP measurements. More than five independent
727 cells and twenty adhesions were picked for each condition. The bracket after the fitting value denote 95%
728 confidence interval of the fitting parameters. In the Frap experiment, Piezo1 is either co-expressed with
729 Integrin β3 or Paxillin.

730 Figure 2

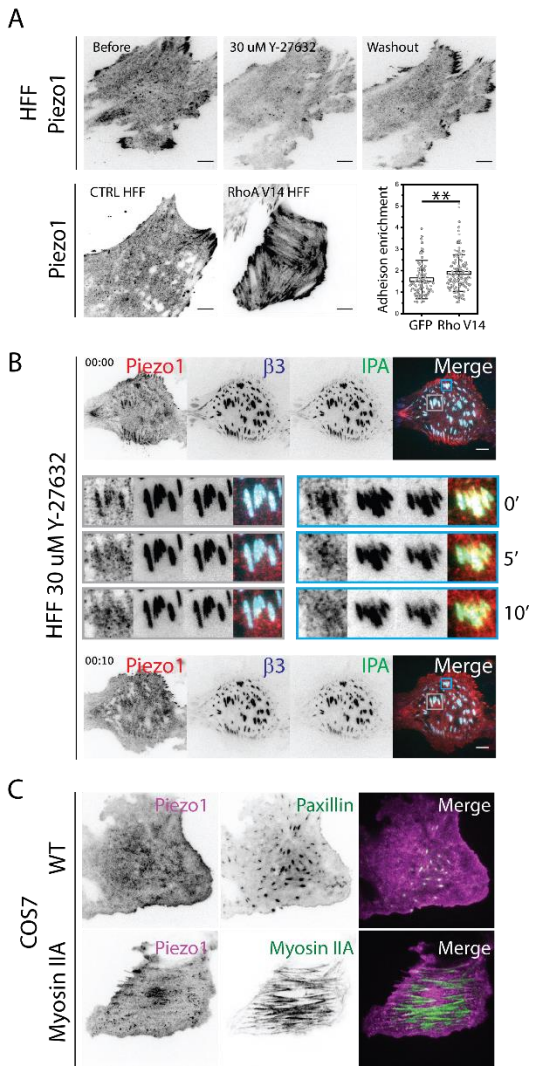

731

732 **Figure 2. Piezo1 localization in HFF cells is controlled by contractility.** (A) Upper panel: Distribution of
733 Piezo1-mRuby3 in HFF cells 15 min after treatment with 30 µM Y-compound and 30 min after washout.
734 Experiments were repeated on > 5 cells with similar results. Lower panel: representative Piezo1 localization
735 and Piezo1 adhesion enrichment quantification in control HFF cells and HFF cells expressing constitutive-
736 active RhoA V14 mutant. Scale bars denote 10 µm. (B) Time-lapse image of HFF cells transfected with
737 Piezo1-mruby3, integrin β3-Emerald and IPA-GFP with the addition of 30 µM Y-27632. Experiments were
738 repeated on > 3 cells with similar results. (C) Fluorescence image of Piezo1-GFP in COS7 cells with/without
739 overexpressing myosin IIA-mCherry.

740 Figure 3

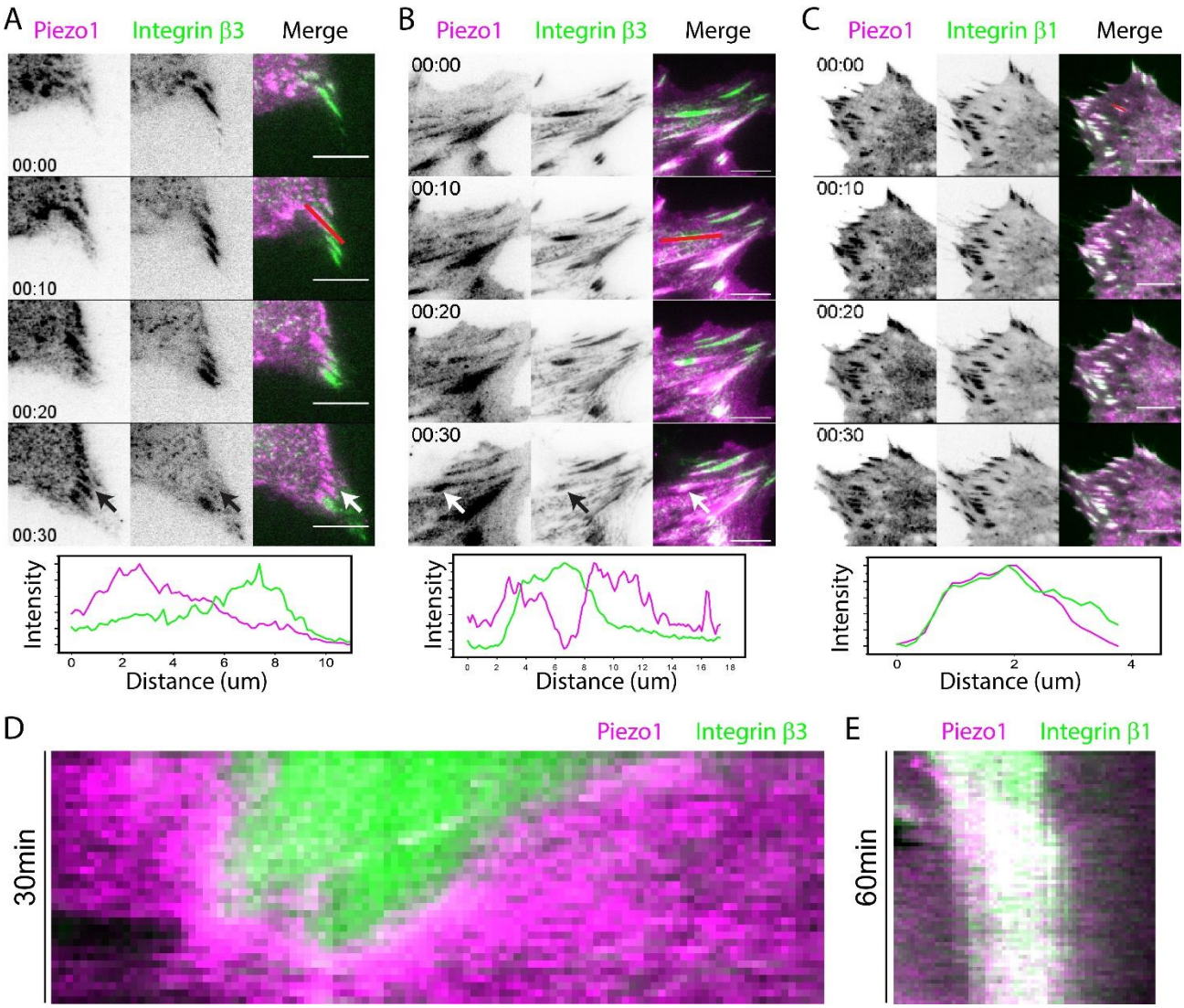

741

742 **Figure 3. Piezo1 recruitment of adhesions precede integrin β3 disassembly.** (A-C) Timelapse of HFF cells
743 co-transfected with Piezo1-mruby3 and mEmerald-Integrin β3 spreading on fibronectin surfaces.A: A
744 spreading cell one hour after seeding. B: A polarized cell after overnight seeding. (C) Timelaspe of HFF cells
745 transfected with Piezo1-mruby3 and mEmerald-Integrin β1 spreading on fibronectin surfaces overnight. The
746 normalized intensity profile of adhesions highlighted by the red line were shown below the figure. (D)
747 Kymograph of Piezo1 and Integrin β3 dynamics of the focal adhesion marked by red line in panel B. (E)
748 Kymograph of Piezo1 and Integrin β1 dynamics of the focal adhesion marked in red in panel C.

749 Figure 4

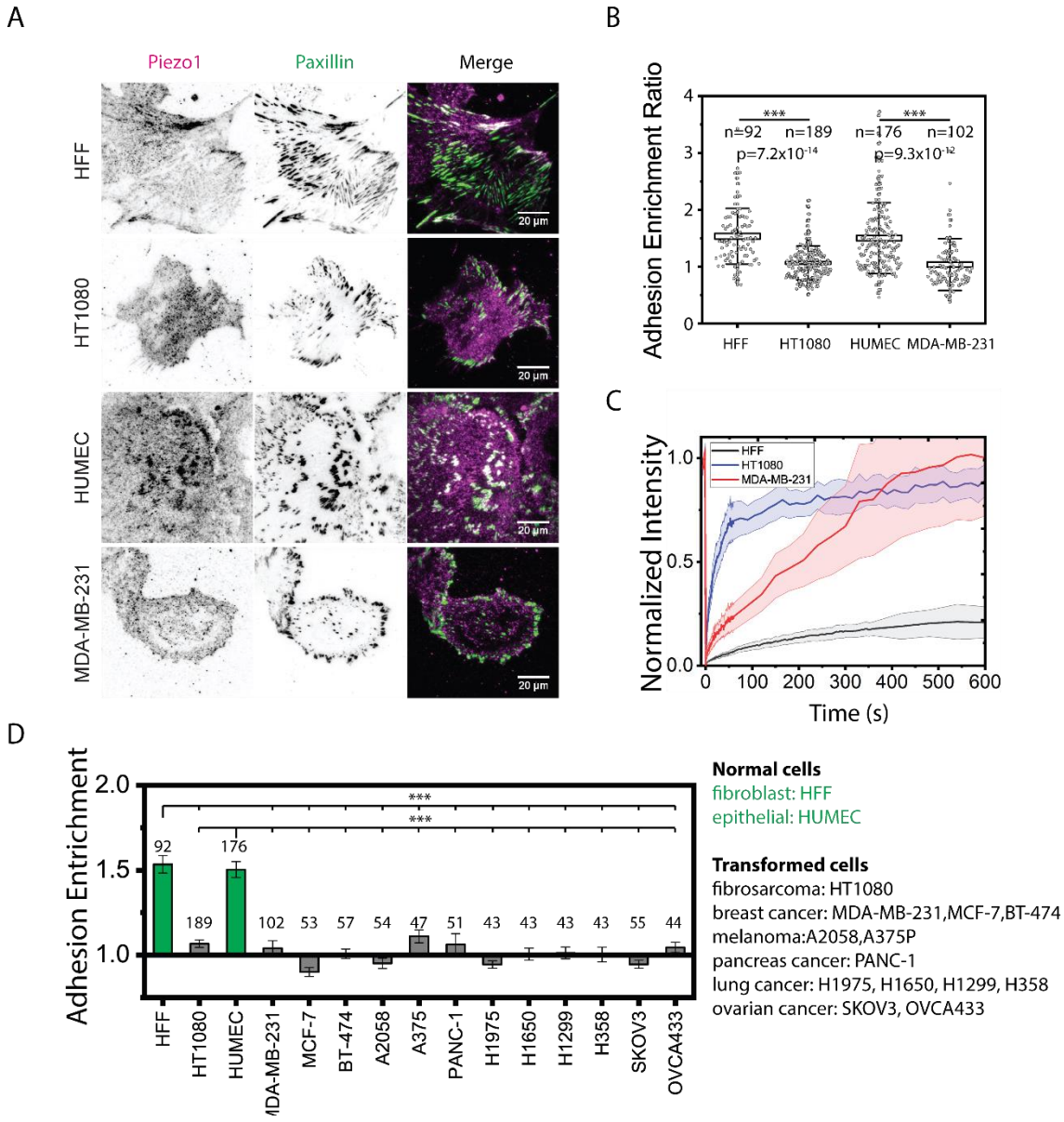

750

751 **Figure 4. Piezo1 localizes to the adhesions of non-transformed cells but is diffusive in transformed**

752 **cells.** (A) Immunostaining of Piezo1 localization in paired normal and transformed cell lines with similar

753 orgin. (B) Quantification of Piezo1 adhesion enrichment for cells in Figure (A). p-values were calculated using

754 two-sample t-test. (C) FRAP recovery curve of Piezo1 in HFF cells and transformed HT1080 and MDA-MB-231

755 cells. The error bar denotes 95% confidence interval of the mean. (D) Quantification of adhesion

756 entrichment of Piezo1 across various normal and transformed cancer cell lines. Error bars denote standard

757 error of the mean. There were statistically significant differences (p-value < 0.001) between HFF/HUMEC and

758 all the cancer cells.

759

760 Figure 5

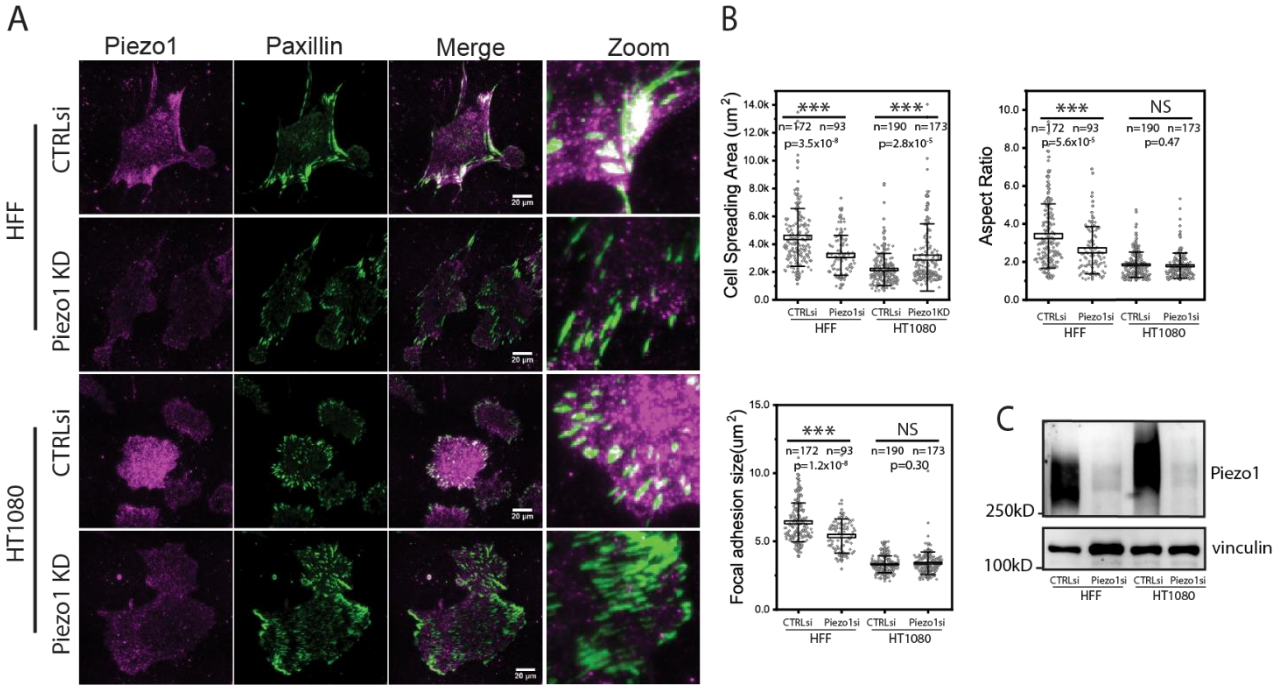

761

762 **Figure 5. Piezo1 localization affects adhesion maturation and correlates with transformation states of**

763 **cells.** (A) TIRF image of fixed cell staining of non-transformed HFF cell line and transformed fibrosarcoma

764 HT1080 with/without Piezo1 knock down after overnight spreading on fibronectin surfaces. Scale Bars

765 denote 20 um. (B) Box plots of the cell spreading areas, cell aspect ratio and mean adhesion sizes of the cells

766 in figure A. Box and error bar denotes the s.e.m and s.t.d of the measurements. The significance value were

767 calculated using two sample t-tests. (C) Western blots of Piezo1 level in control siRNA and piezo1 knock-

768 down cells.

769

770 Figure 6

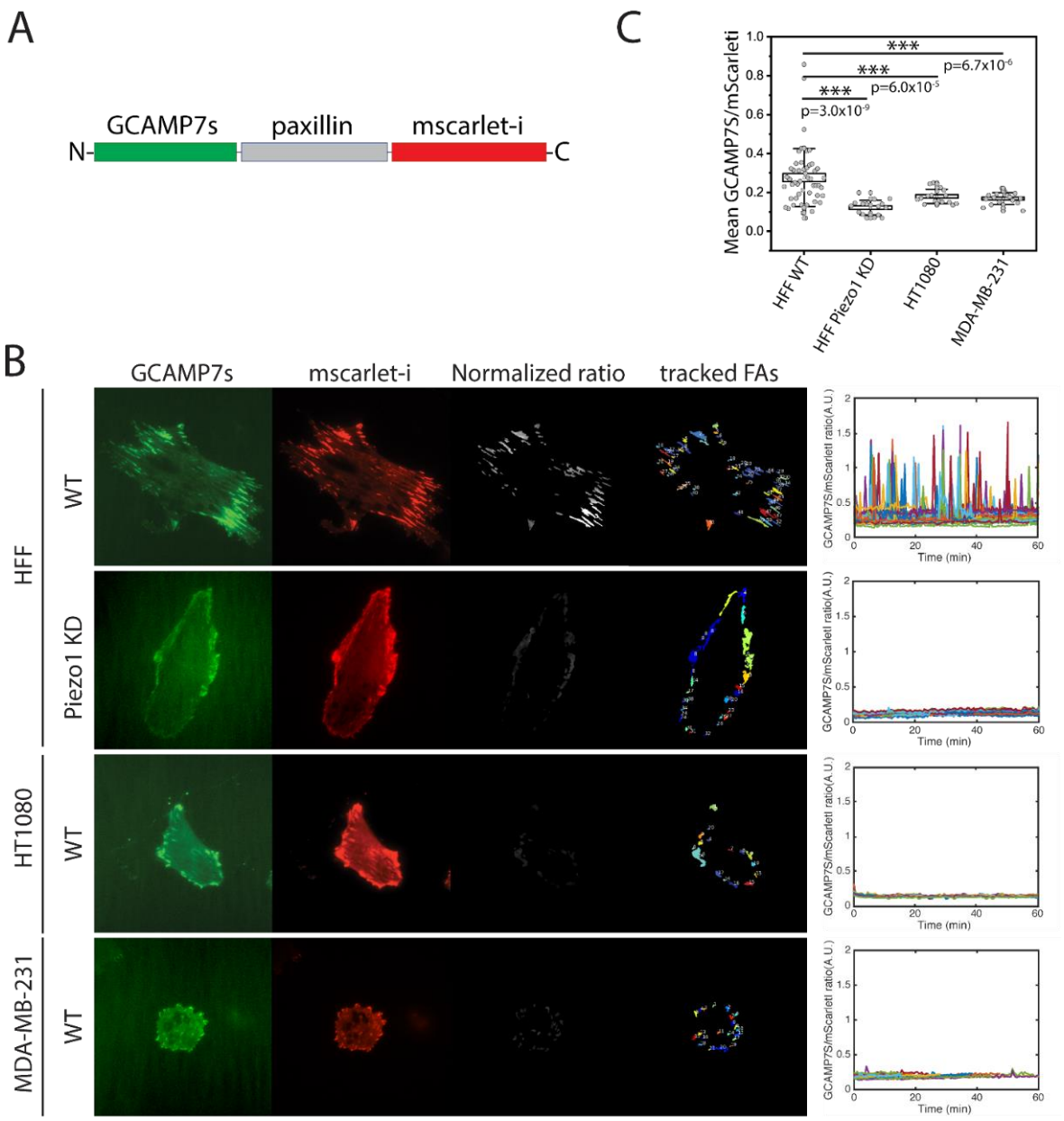

771

772 Figure 6. Normal and transformed cells have distinct adhesion calcium signals . (A) Domain Illustration of

773 the novel adhesion targeting calcium sensor based on jGCaMP7s from Janelia. (B) Left: TIRF image montages

774 of representative HFF cells (with/without Piezo1 knock down), HT1080 and MDA-MB-231 cells transfected

775 with paxillin calcium sensor. The cells were seed on fibronectin surfaces overnight before imaging.

776 Normalized ratio represents the ratio image between jGCaMP7s and mScarlet-I, which is an measure of local

777 Ca^{2+} concentrations. Right: calcium level fluctuations over time in the tracked adhesions of the cell presented

778 in the left panel, each line in the image denotes a single adhesion. The interval of measurement is 30 s. (C)

779 Quantification of average calcium ratio in tracked adhesions over 60 min for different cell types.

780

781 Figure 7

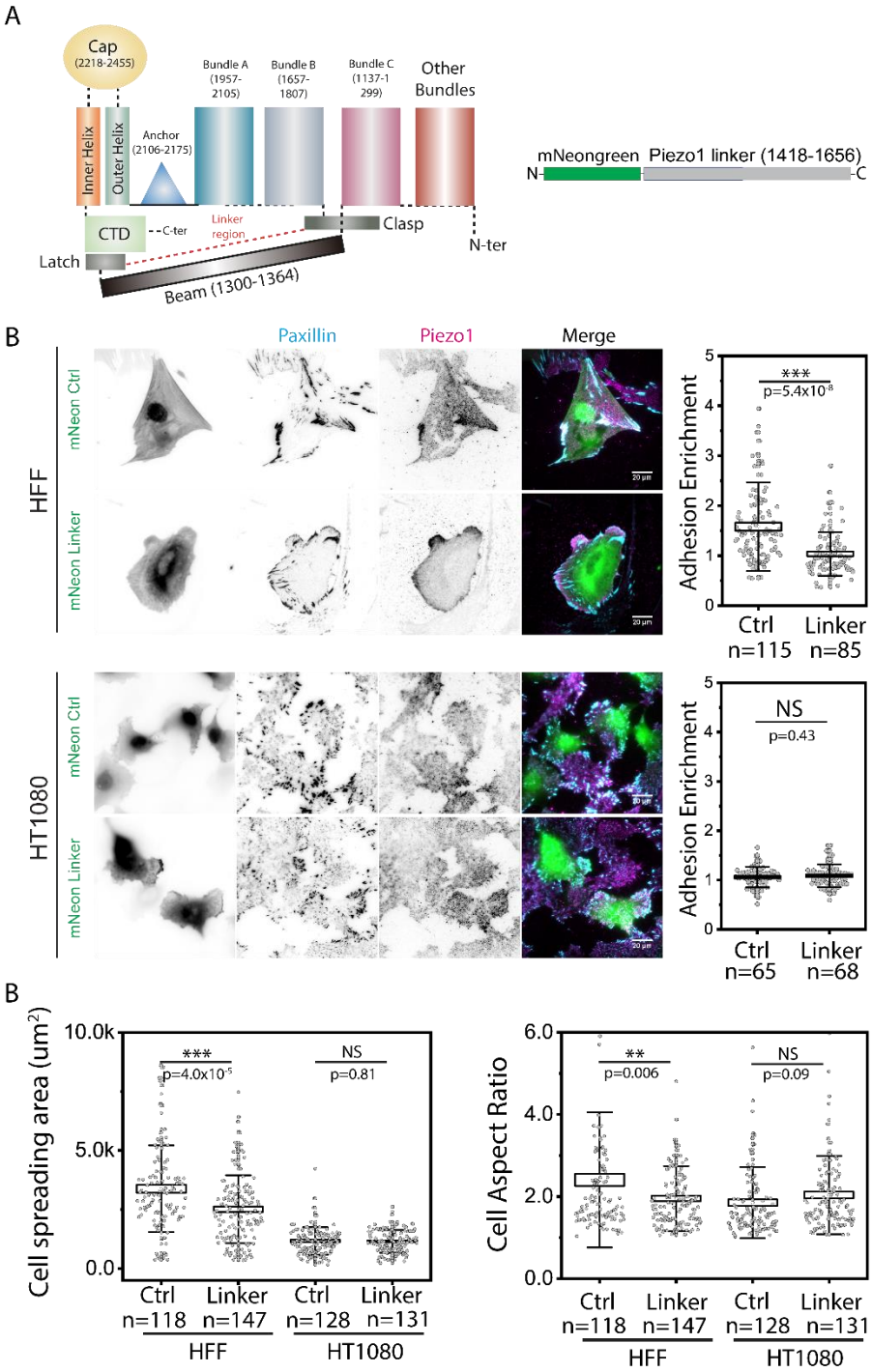

782

783 Figure 7, The linker domain of Piezo1 is linked to adhesion recruitment and alters cell morphology in HFF

784 cells. (A) Domain map of Piezo1 and the long-linker construct. The residue number is based on mouse Piezo1

785 structures . (B) Immunostaining of HFF and HT1080 cells transfected with mNeongreen control vector or

786 mNeongreen labeled Piezo1 linker construct. The cells were seeded on fibronectin surface overnight and

787 stained with paxillin and Piezo1. (C) Box plot of cell spreading area and cell aspect ratio of positively

788 transfected cells. Box and error bar present s.e.m and s.t.d respectively. Statistical significance were

789 calculated using two sample t-test.

790

791 Figure 8

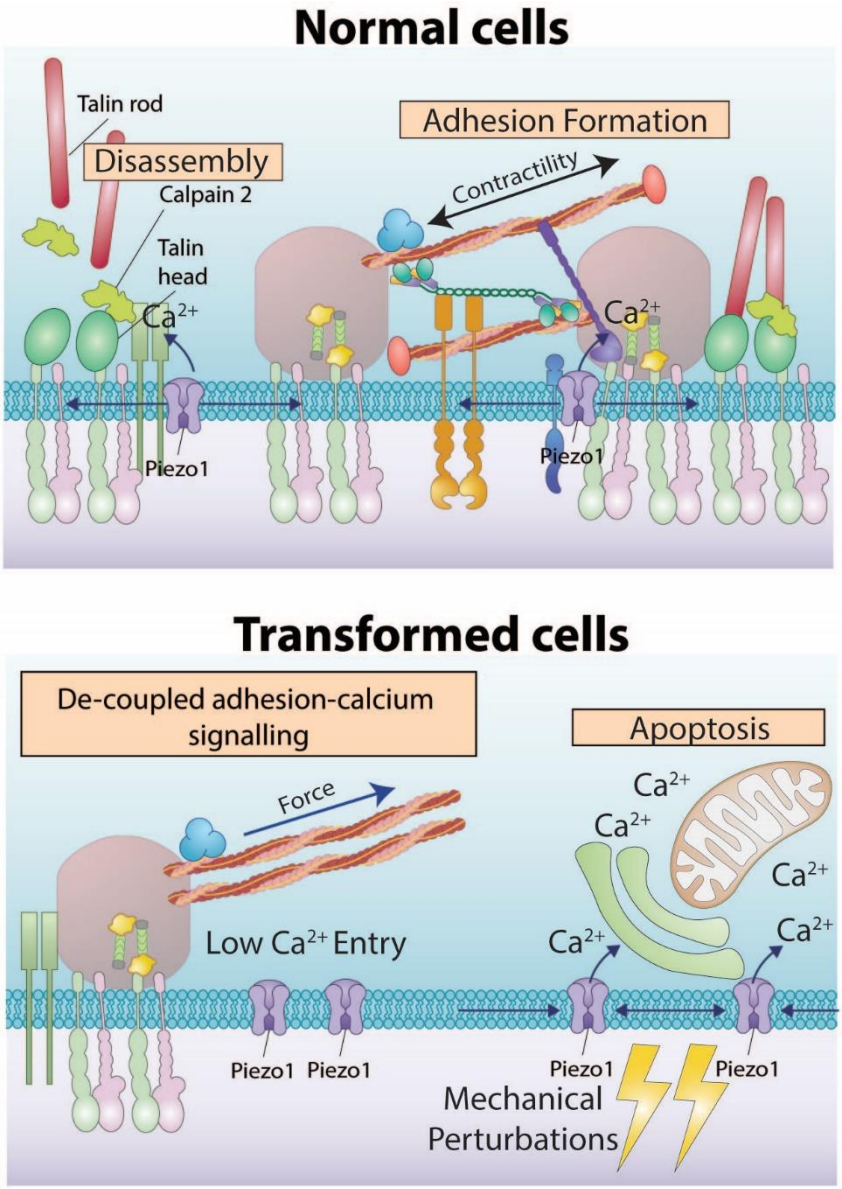

792

793 **Figure 8, Model of Piezo1's regulation in normal and transformed cells.** (Top Panel) In normal cells, Piezo1
794 is recruited to maturing focal adhesions in a force dependent manner, where it regulates both the growth
795 and turnover of focal adhesions. (Bottom Panel) In transformed cells Piezo1's localization is diffusive and it
796 no-longer regulate adhesion morphology, which might contribute to the mis-regulated calcium signaling
797 observed in cancer cells including stretch dependent apoptosis(*16*).

798

799 *Supplementary Figures*

800 *Figure S1*

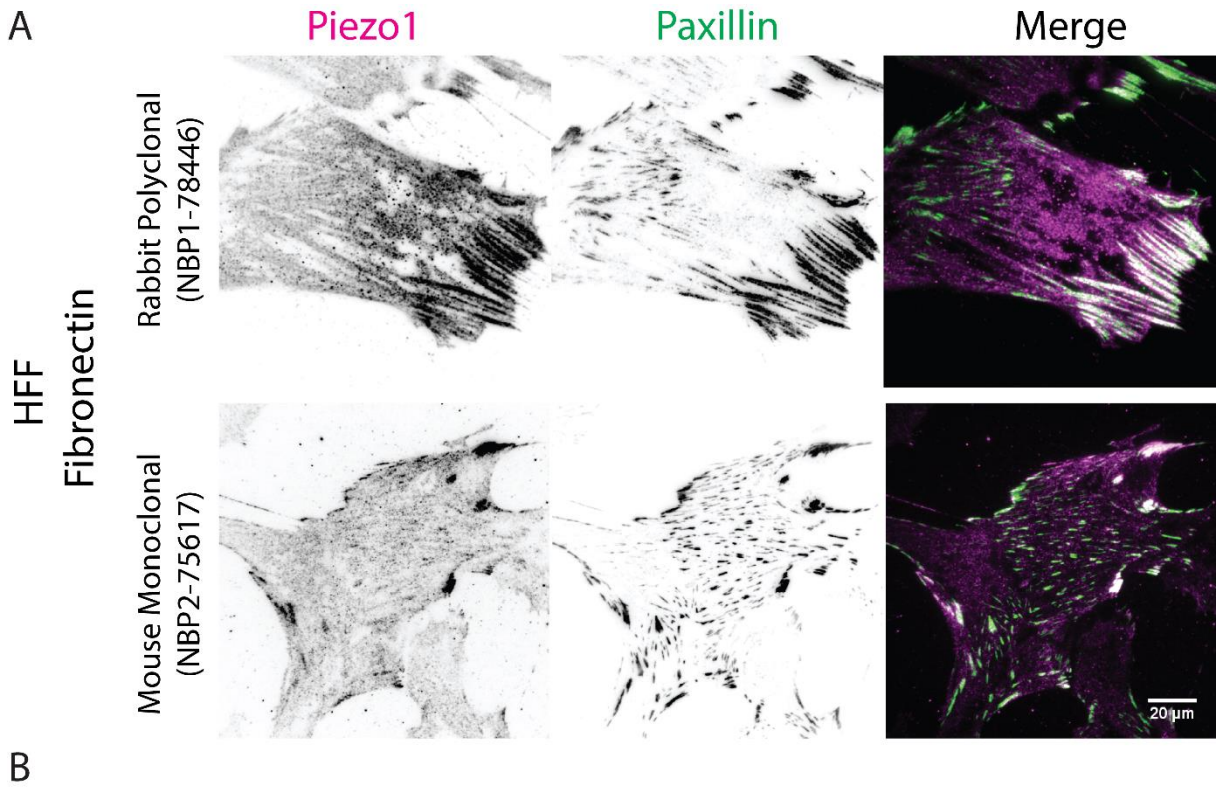

Target Sequence :	GCAAGTTCGTGCGCGGATT
siRNA sense sequence :	GCAAGUUCGUGCGCGGAUUdTdT
siRNA antisense sequence :	AAUCCGCGCACGAACUUGCdTdT

801

802 **Figure S1, Immunostaining of Piezo1 localization of HFF cells.** (A) HFF cells were seeded on fibronectin
803 surfaces overnight, fixed with paraformaldehyde and stained for Piezo1 with two validated Piezo1 antibody
804 and paxillin. (B) Sequence information of Piezo1 siRNA used in the study (SASI_HS01_00208585 from Merck
805 Sigma-Aldrich).

806 *Figure S2*

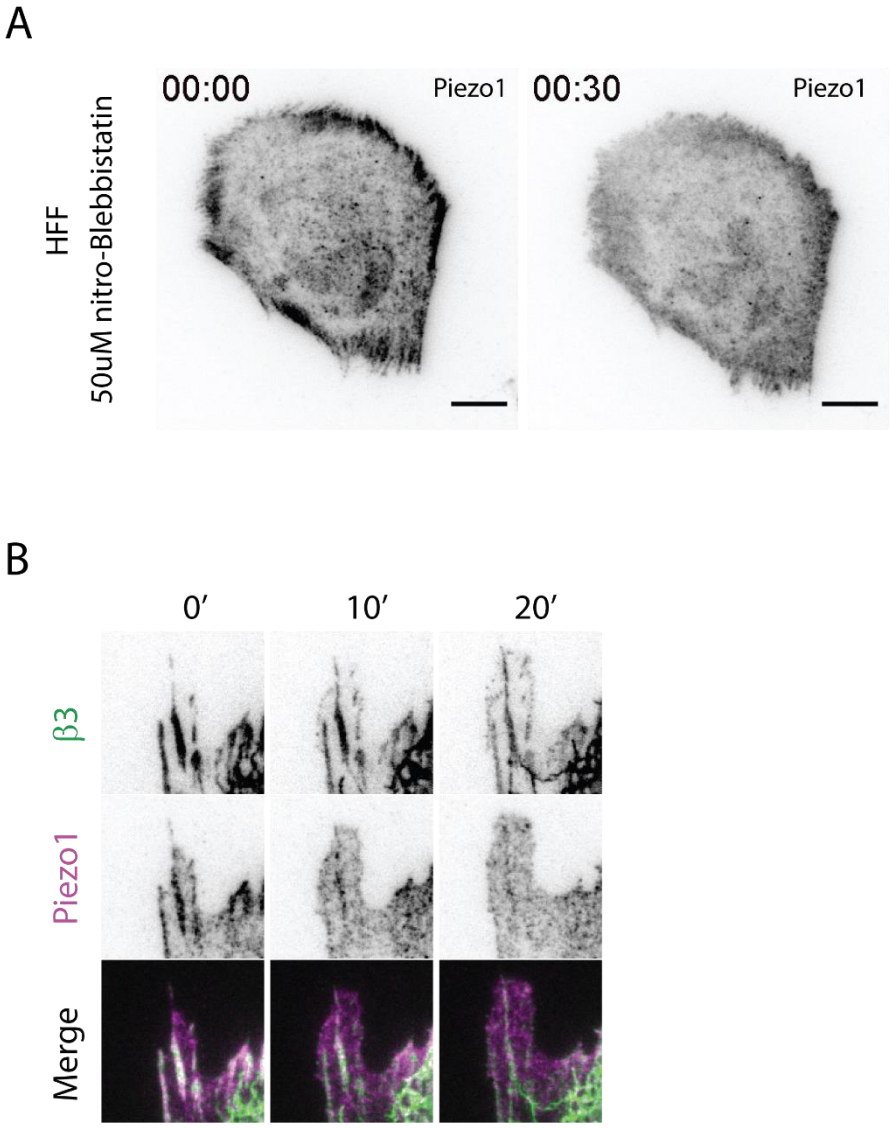

807

808 **Figure S2.** (A) HFF cells transiently transfected with Piezo1-mruby3 were treated with 50 µM nitro-
809 Blebbistatin at time 0. After 30 min incubation, the localization of Piezo1 at focal adhesions were lost. Scale
810 bars denote 10 µm. (B) HFF cells transiently transfected with mEmerald-integrin β3 and Piezo1-mruby3 were
811 pre-treated with 2.5 µM PTP-PEST inhibitor that inhibits adhesion turnover by phosphatases before addition
812 of 20 µM Y-27632. In this condition, Piezo1 dissociated from adhesions before integrin β3 upon tension release.

813

814 *Figure S3*

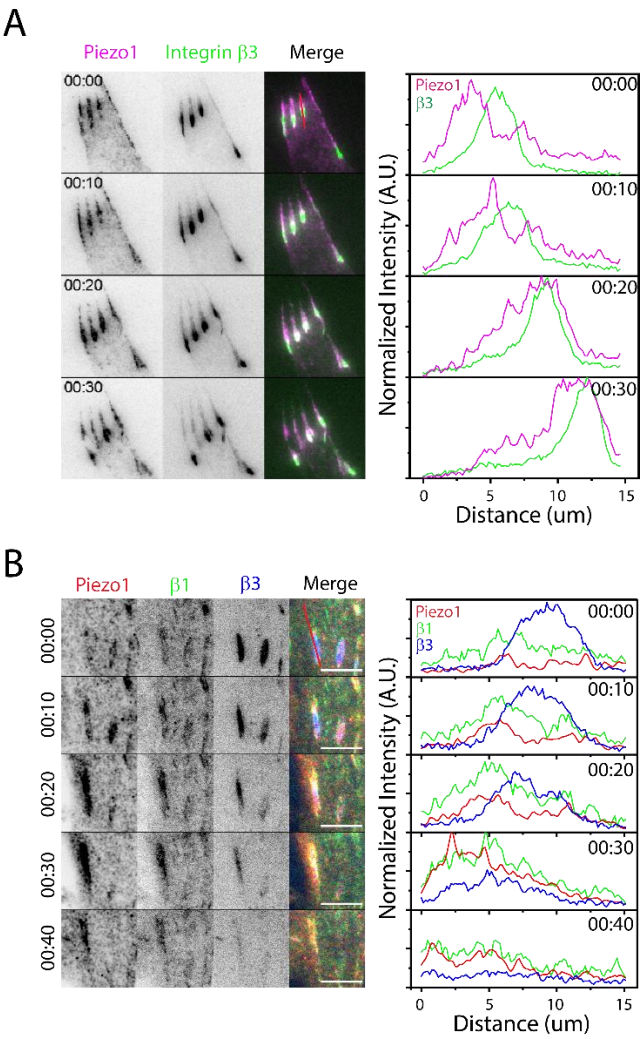

815

816 **Figure S3. Dynamics of Piezo1 localization in relation to integrins.** (A) Adhesion time lapse HFF cells
817 transiently transfected with mEmerald-integrin β3 and Piezo1-mruby3. The right panel showed normalized
818 intensity profiles of the adhesions marked by red line over time. (B) Adhesion time lapse of HFF cells
819 transfected with BFP-integrin β3, mEmerald-integrin β1 and Piezo1-mruby3. The right panel showed
820 normalized intensity profiles of the adhesions marked by red line over time. The normalizations were done by
821 dividing the intensity profiles by the maximum intensity value observed for each protein in the whole time
822 series. Scale Bars denote 10 µm.

823 *Figure S4*

824

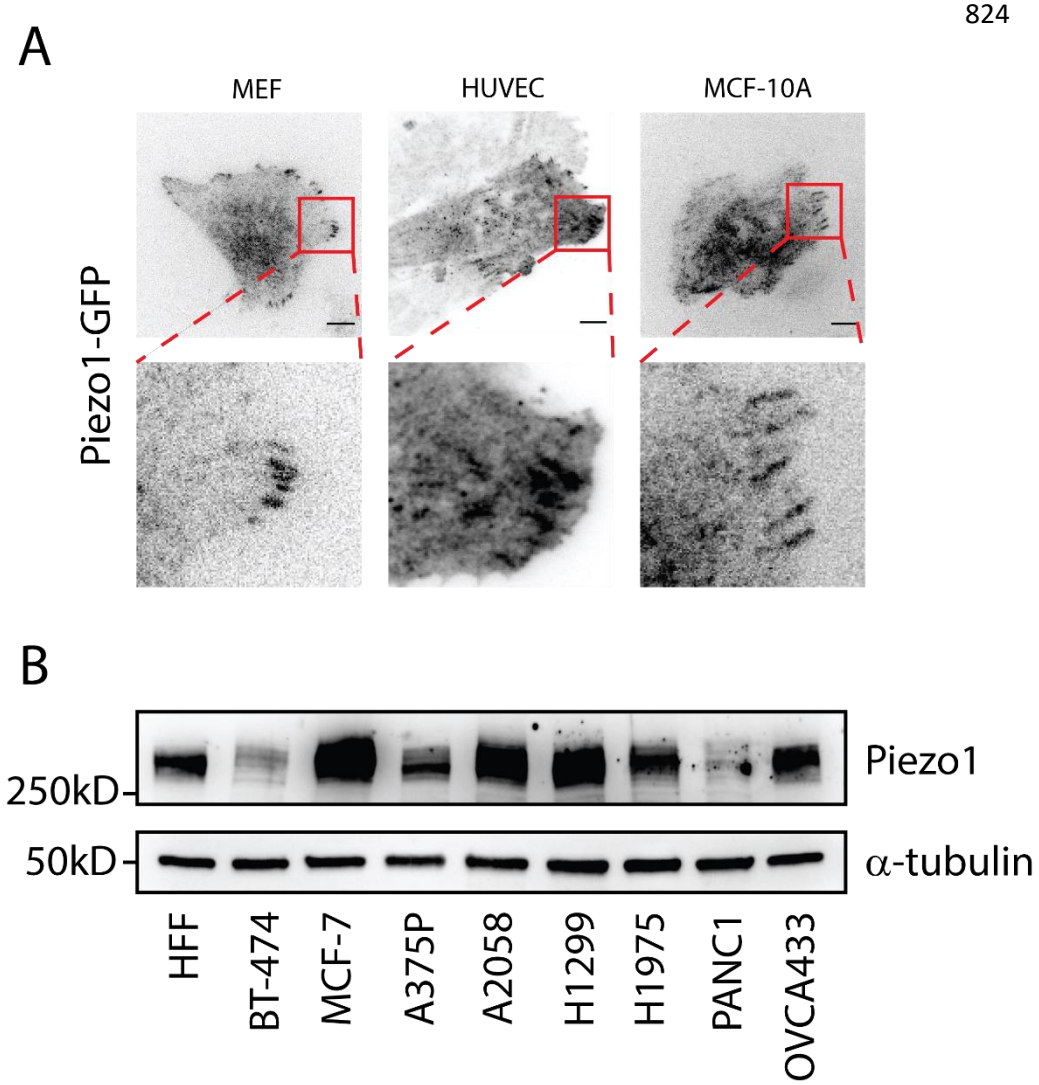

825

826 **Figure S4** (A) TIRF live images of Piezo1-GFP localization in more normal cell lines tested. (B) Western blot
827 images of Piezo1 expression in various cancer cell lines compared against HFF cells.

828

829 *Figure S5*

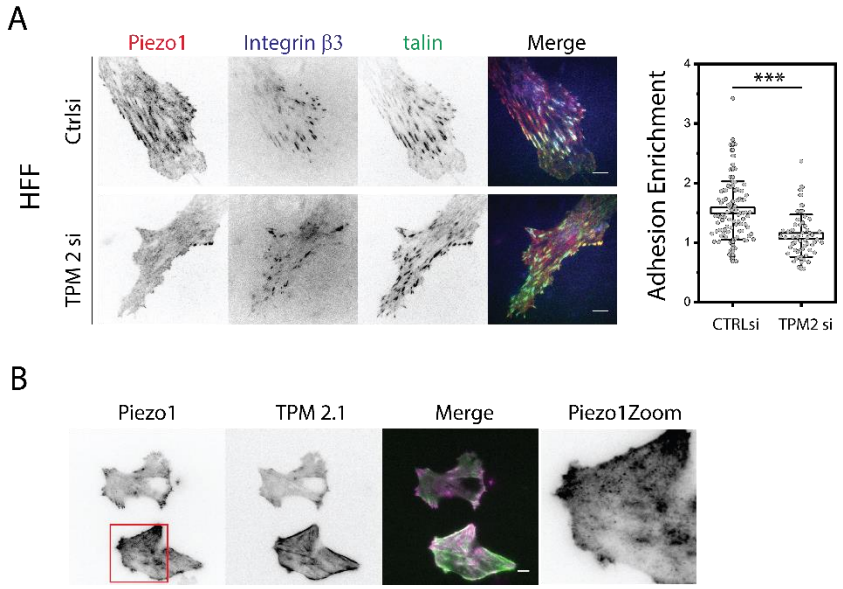

830

831 **Figure S5. Piezo1 localization in cells with altered transformation state.** (A) Representative HFF cells with
832 Control siRNA and TPM 2.1 siRNA knock down were transfected with Piezo1-mruby3, Integrin β3-BFP and
833 talin-GFP. The cells were seeded on fibronectin surfaces overnight and imaged by TIRFM. Right Panel:
834 quantification of adhesion enrichment with Ctrlsi and TPM 2.1 si (C) Transient expression of TPM 2.1 -YFP in
835 MDA-MB-231 cells led to the recruitment of Piezo1 to the end of stress fibres decorated by TPM 2.1 (TOP
836 panel). The images present representative cells out of > 20 imaged. Scale Bars denote 10 um.

837

838 *Figure S6*

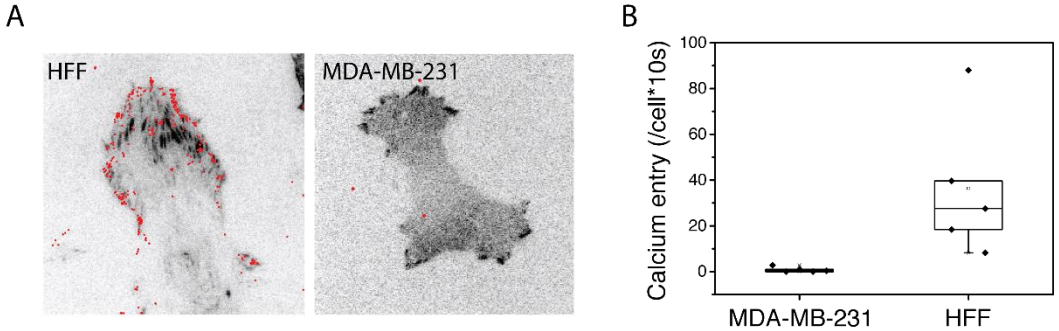

839

840 **Figure S6 HFF and MDA-MB-231 cells showed distinct local calcium entry pattern**. (A) Locations of local
841 calcium entry events (marked by red dots) in HFF cells and MDA-MB-231 cells measured at 100 frames/s for
842 50s, overlaid with focal adhesions marked by paxillin. Significantly more local calcium signal is observed in HFF
843 cells. (B). Box plot of the rate of local calcium events per cell for HFF and MDA-MB-231 cells. Each point
844 denotes an independent cell.

845

846

847

848 *Figure S7*

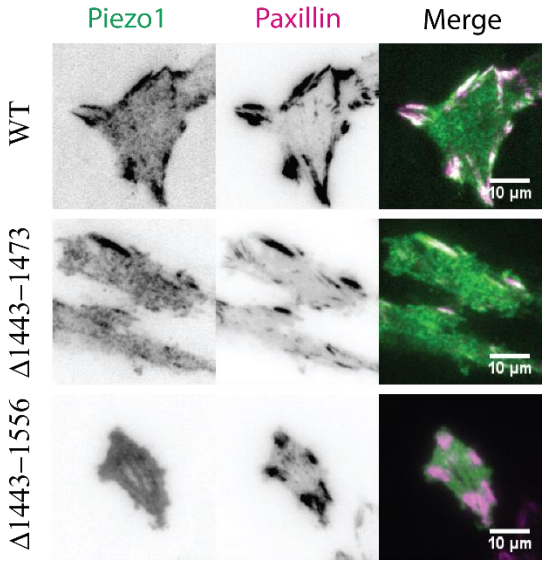

849

850 **Figure S7 Linker domain mutants of Piezo1**. Representative images of FAK-/- MEF cells transfected with
851 paxillin-mapple and wild type/linker deletion mutant of Piezo1. Similar behavior were observed in 3 biological
852 repeats with > 10 cells for each condition.

853

854 *Figure S8*

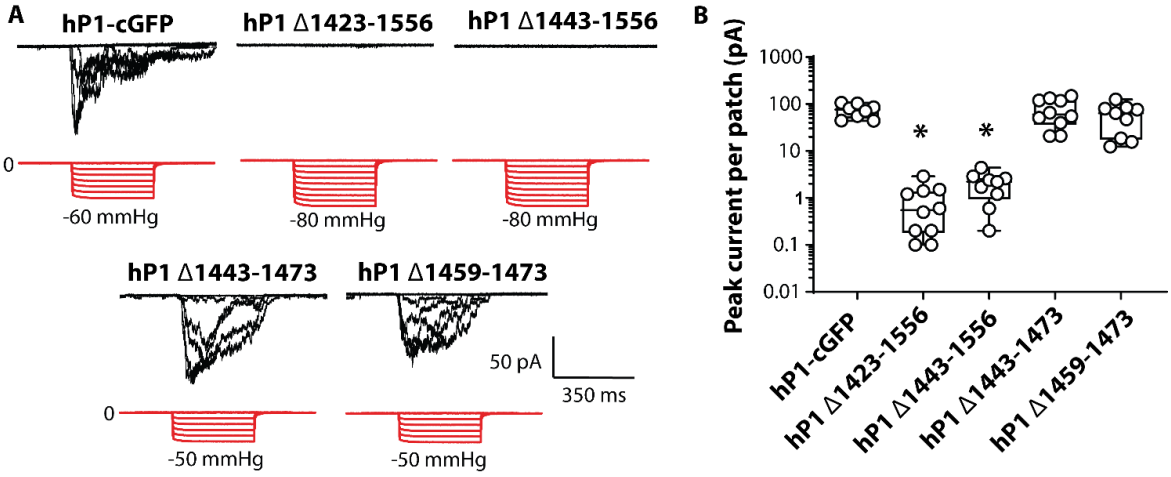

855

856 **Figure S8. Determination of stretch activation of Piezo1 deletion mutants.** (A) Representative patch-
857 clamp traces from human Piezo1 c-terminal EGFP fusion (hP1-cGFP) in cell-attached patches at -60 mV holding
858 potential expressed in Piezo1 KO HEK293T cells compared to four deletion mutants. Current traces are shown
859 in black and square wave negative pressure pulses increasing from 0 mmHg in increments of -10 mmHg are
860 shown in red with the peak negative pressure documented for clarity. (B) Box and whiskers plots indicating
861 the peak current elicited per patch from negative pressure application with all mutant Piezo1 channels. *
862 represents statistical significance from hP1-cGFP using one-way ANOVA with Dunnett's post hoc test.

863

864